

ARTICLE

Stages of Embryonic Development in the Amphipod Crustacean, *Parhyale hawaiiensis*

William E. Browne,¹ Alivia L. Price,^{1,2} Matthias Gerberding,² and Nipam H. Patel^{2*}

¹University of Chicago, Department of Molecular Genetics and Cell Biology, Committee on Developmental Biology, Chicago, Illinois

²University of California – Berkeley, Departments of Molecular Cell Biology, Integrative Biology, Center for Integrative Genomics, and HHMI, Berkeley, California

Received 1 March 2005; Accepted 12 May 2005

Summary: Studying the relationship between development and evolution and its role in the generation of biological diversity has been reinvigorated by new techniques in genetics and molecular biology. However, exploiting these techniques to examine the evolution of development requires that a great deal of detail be known regarding the embryonic development of multiple species studied in a phylogenetic context. Crustaceans are an enormously successful group of arthropods and extant species demonstrate a wide diversity of morphologies and life histories. One of the most speciose orders within the Crustacea is the Amphipoda. The embryonic development of a new crustacean model system, the amphipod *Parhyale hawaiiensis*, is described in a series of discrete stages easily identified by examination of living animals and the use of commonly available molecular markers on fixed specimens. Complete embryogenesis occurs in ~250 h at 26°C and has been divided into 30 stages. This staging data will facilitate comparative analyses of embryonic development among crustaceans in particular, as well as between different arthropod groups. In addition, several aspects of *Parhyale* embryonic development make this species particularly suitable for a broad range of experimental manipulations. *genesis* 42:124–149, 2005. © 2005 Wiley-Liss, Inc.

Key words: Crustacean; amphipod; arthropod; evolution; development; embryogenesis; segmentation; Engrailed; Distalless

INTRODUCTION

The fields of development, genetics, and evolution have advanced dramatically in the past 25 years. This is in large part due to forward genetics approaches in such species as *Drosophila melanogaster* and *Caenorhabditis elegans*. The information gathered from this work has given us insight into developmental mechanisms and their underlying genetic architecture. Only a few additional animal taxa (such as *Xenopus laevis*, *Gallus domestica*, *Mus musculus*, *Danio rerio*) have come under the intense scrutiny received by *Drosophila* and

C. elegans. Thus, many critical questions remain with regard to how evolution operates over time and how it has come to generate the full range of extant biological diversity. Although we have accumulated significant data in model species, we are currently left with more questions than answers regarding the tempo and mode of evolutionary change due to the vast evolutionary distances between the current model systems. This information deficit is largely due to the paucity of developmental, genetic, and evolutionary data available in nonmodel organisms. The descriptive analyses of gene expression in a wide range of taxa are still relatively few in number. Likewise, our ability to examine the functional basis of observed changes in gene expression is restricted to a few species. This problem can be addressed by “filling in the gaps” with new model systems more closely related to the current systems used by researchers. Indeed, the ultimate goal should be to “cover” the Tree of Life with a sufficient spread of well-studied taxa that the process of evolution can be approached and studied with several levels of resolution in all major organismal lineages. Ideally, these new taxa should be systems in which embryos are readily obtainable year-round and permit the design and implementation of functional studies with relative ease.

Several recent studies have examined the evolutionary relationships among the major groups of arthropods. The data suggest two possible relationships between the Insecta (hexapods) and the Crustacea. One possibility is that the two groups are sister taxa (Boore *et al.*, 1995, 1998; Friedrich and Tautz, 1995; Eernisse, 1997; Giribet *et al.*, 2001). The other possibility is a “Pancrustacea”

Present address for W.E. Browne: Kewalo Marine Lab, University of Hawaii.

Present address for M. Gerberding: Max-Planck-Institut für Entwicklungsbiologie, Tübingen, Germany.

*Correspondence to: M. Gerberding, University of California, Berkeley, Department of Integrative Biology, 3060 VLSB # 3140, Berkeley, CA 94720-3140.

E-mail: nipam@uclink.berkeley.edu

Published online in Wiley InterScience (www.interscience.wiley.com).

DOI: 10.1002/gene.20145

clade in which the insects branch from within the Crustacea (Regier and Shultz, 1997; Hwang *et al.*, 2001). In this scenario the insects would represent a terrestrialized branch of crustaceans. In either case the crustaceans form a key outgroup to the insects and in this context will help enormously in our understanding of arthropod evolution. The amphipod *Parhyale hawaiiensis* (Dana, 1853) is a crustacean species that is particularly well suited for developmental, genetic, and evolutionary analysis and has the potential of filling an important taxonomic gap in current comparative studies.

While detailed staging information is available for *Drosophila* (Campos-Ortega and Hartenstein, 1985; Hartenstein, 1993), only relatively simple staging systems exist for the crustaceans *Cherax* (Sandeman and Sandeman, 1991), and *Nebalia* (Olesen and Walossek, 2000). Amphipods (Peracarida; Malacostraca; Crustacea) have been the subject of study by developmental biologists since the late 19th century (e.g., Langenbeck, 1898; Weygoldt, 1958). However, detailed descriptive staging information covering the complete course of embryogenesis in any amphipod is largely lacking. Commonly referred to as beachhoppers or scuds, amphipods are malacostracan crustaceans and thus closely affiliated with more familiar Crustacea such as krill, lobsters, and crabs. Within the Crustacea, amphipods rank as one of the most ecologically successful and speciose extant orders and occur in nearly all known marine, fresh, and brackish water environments as well as in high humidity terrestrial ecosystems (such as tidal zones, coastal flood plains, and forest leaf litter) (e.g., Barnard and Karaman, 1991; Vinogradov *et al.*, 1996; also Lindeman, 1991; Sherbakov *et al.*, 1999; Kamal'tynov, 1999; Vainola and Kamal'tynov, 1999; Sheader *et al.*, 2000; Poltermann *et al.*, 2000; Gasca and Haddock, 2004). They have predominately exploited scavenging niches and thus an apt analogy for the group would be "the flies of the sea." This ecological diversity is matched by a high level of morphological diversity. Several thousand amphipod species have been described and the current rate of several new species descriptions per year suggests that the upper limit of extant species is far higher than the current species count.

Importantly, several aspects of *Parhyale hawaiiensis* life history make this particular species amenable to many types of classical and modern laboratory analyses and techniques. *Parhyale hawaiiensis* are detritivores that have a circumtropical, worldwide, intertidal, and shallow water marine distribution (Shoemaker, 1956; Barnard, 1965), possibly as a species complex (Myers, 1985). They have been reported to aggregate in large populations (>3,000/m²) on decaying mangrove leaf material in environments subjected to rapid changes in salinity (Poovachiranon, 1986). The ability to tolerate the rapid temperature and osmotic changes that occur in their preferred shallow-water habitat allows this robust species to thrive under typical laboratory conditions. Females brood their young in a ventral pouch and produce embryos every 2 weeks once they reach sexual

maturity. Fertilized eggs can be removed from females prior to their first cleavage and are sufficiently large to perform microinjections (Gerberding *et al.*, 2002) and blastomere isolations (Extavour, 2005) with relative ease. Eggs collected can be hatched individually and the mature animals can subsequently be used in pairwise sister-brother or mother-son matings to generate inbred lines. The length of embryogenesis is relatively short, lasting roughly 10 days. Interestingly, the *P. hawaiiensis* body plan is established by distinct and invariant cell lineages very early in embryogenesis (Gerberding *et al.*, 2002).

***Parhyale hawaiiensis* Body Plan**

The basic body plan of *P. hawaiiensis* follows that of the typical arthropod in that the ground plan is organized around a series of repeating segmental units along the anterior-posterior (A-P) axis. Several synapomorphic characters clearly unite the Amphipoda (Schram, 1986; Schmitz, 1992). Most recognizable among these characters are the lateral compression of the body, sessile compound eyes, and the relative orientation of the pereopods (appendages of thoracic segments T4-T8) to the body axis (pereopods of T4 and T5 orient anteriorly, pereopods of T6-T8 orient posteriorly, thus the name for the group, amphipod) (Fig. 1). Additionally, amphipods have large coxal plates (expanded plates attached dorsally to the base of thoracic appendages) (Fig. 1).

Typical of most amphipods, the *P. hawaiiensis* cephalon (head) is composed of the anteriormost six segments. The anteriormost preantennal segment bears no paired appendage. The remaining five segments do possess paired appendages. From anterior to posterior, the paired appendages of the head are the uniramous first antenna (An1), uniramous second antenna (An2), gnathobasic mandibles (Mn), biramous first maxillae (Mx1), and the biramous second maxillae (Mx2). In addition, the first thoracic segment (T1) is fused to the cephalon. The T1 appendage pair, the maxillipeds, are triramous, fused at their base, and extensively modified to assist in feeding (Fig. 1). There is a close arrangement of the gnathal appendages, including the maxillipeds, in a basket shape around the mouth to form a highly compact buccal mass (Fig. 1b).

The next seven segments of the thoracic region, the second through eighth thoracomeres (T2-T8), each articulate independently and bears a pair of appendages. The T2-T6 appendages possess a modified dorsal appendage branch, an epipod, that articulates underneath the animal posteriorly, medially, and ventrally as a thin, laterally flattened sheet that functions as a respiratory organ (Divakaran and Pillai, 1975, 1981) (Fig. 11). Sexually mature females possess an additional ventral appendage branch, termed an oostegite, on appendages T2-T5 that interlock to form the protected ventral brood pouch into which fertilized eggs are shed and incubated until hatching (Fig. 1b). The T2 and T3 appendages, termed gnathopods, are subchelate and function in grasping and mating. The T3 appendage is

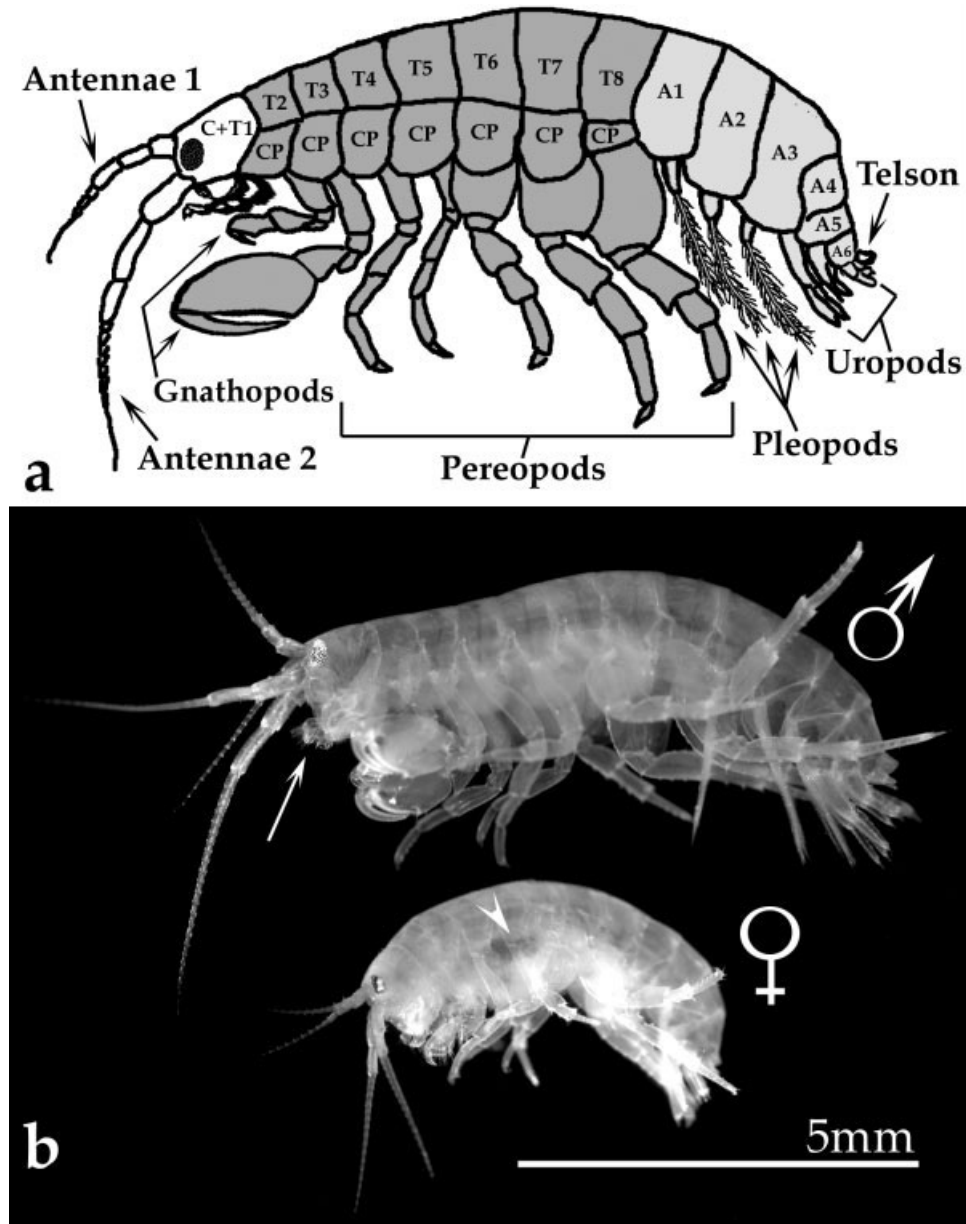


FIG. 1. The *Parhyale hawaiiensis* body plan. **a:** Schematic of the adult body plan. By convention the head (white) consists of the first six segments (termed the cephalon) plus the first segment of the thorax (T1). All segments from the second cephalic segment posterior bear a pair of appendages. For the head these appendages from anterior to posterior are as follows: antennae 1 (An1), antennae 2 (An2), mandibles (Mn), first maxillae (Mx1), second maxillae (Mx2), and the maxillipeds of the first thoracic segment (T1). The pereon, composed of T2–T8, is colored dark gray. Each thoracic segment of the pereon possesses a pair of appendages and the proximal-most element of each appendage, the coxa, has a dorsal branch which is compressed and expanded into a structure called the coxal plate (CP). The appendages of T2 and T3 are distinctly subchelate (clawed) in form and termed gnathopods. The gnathopod of T3 is sexually dimorphic; in mature males it is greatly enlarged (compare male to female in **b**). T4–T8 possess appendages termed pereopods. The abdominal segments A1–A6 are colored light gray. A1–A3 form the pleon, and each bears a pair of appendages termed pleopods. The final three segments of the abdomen (A4–A6) form the urosome, and each of these segments bears a pair of appendages termed uropods. At the very posterior is the telson, which is a cleft flap of cuticle just posterior and dorsal of the anus. **b:** Sexually mature animals possess a number of dimorphic characters. Males are larger than females. The appendages of T3 are greatly enlarged in males. Females possess a ventral brood pouch in which they incubate their eggs until hatching (arrowhead). All amphipods retain a highly compact arrangement of mouthparts termed the buccal mass (arrow).

sexually dimorphic (larger on mature males) (Fig. 1). The T4–T8 appendages, functioning in locomotion, are termed pereopods (Fig. 1).

The abdominal region is composed of the next six segments and is divided into two regions: segments A1–A3 constitute the pleon and segments A4–A6 constitute the

urosome. Each abdominal segment bears a pair of biramous appendages. The appendages of abdominal segments one through three (A1–A3) are termed pleopods and function in both swimming locomotion as well as in moving water over the ventrally located thoracic gills. Each pair of pleopods is fused at its base along the ventral midline of the animal and is highly setose (Fig. 1). The appendages of abdominal segments four through six (A4–A6) are termed uropods. These appendages are reduced, thickened, and bear a number of stout spikes along their proximal–distal axis (Fig. 1). The terminal structure, the telson, is cleft and reduced in size relative to comparable structures of other types of crustaceans.

Staging Methods

We used *in vivo* light microscopy and DAPI visualization of nuclei in fixed embryos to create reference stages of *Parhyale hawaiiensis* embryonic development. *In vivo* staging of living embryos is important for recognition and identification of developmental stages prior to manipulation. Companion DAPI images facilitate staging of manipulated embryos through nuclear staining. Appendage development is included for accurate staging of older embryos and studies specific to appendage development. We also used two antibodies that are broadly cross-reactive across species as molecular markers during *P. hawaiiensis* embryonic development. The product of the segment polarity gene *engrailed* (*en*) is required for proper segmentation in *Drosophila* and exhibits a conserved expression pattern in the posterior compartment of developing segments and appendages in all arthropod species studied thus far. The *en* gene is also expressed in selected sets of cells in the developing CNS (Patel *et al.*, 1989a,b; Duman-Scheel and Patel, 1999). Thus, the cross-reactive anti-*EN* antibody is useful for following the progression of segmentation as well as neurogenesis. The product of the distal appendage patterning gene, *Distalless* (*Dll*), possesses a conserved expression pattern in developing appendages (Panganiban *et al.*, 1997), and thus the cross-reactive anti-*Dll* antibody is useful for following the establishment and development of appendage fields.

RESULTS

Parhyale hawaiiensis (Fig. 1b) is small (<2 cm) and easy to maintain in very dense cultures in the laboratory. They have a high tolerance to variations in water quality, salinity, and temperature. Mature adults breed approximately every 2–3 weeks, year-round. In addition, they have a relatively short egg-to-egg generation time of 7–8 weeks when maintained at 26°C. From egg deposition to egg hatching, embryogenesis takes ~250 h (10 days) to reach completion (Fig. 2). All eggs in a single brood are roughly synchronous in development, as all eggs are deposited within 1 h. The average brood size is six embryos, with a range of as few as one and as many as 25 embryos per ovigerous (egg-bearing) female. As direct developers, the hatchlings possess a complete

complement of segments and appendages morphologically similar to those of adult animals. Females normally brood the embryos in a ventral brood pouch. Embryos can be rapidly and easily removed from the brood pouch and maintained in clean seawater. Furthermore, *P. hawaiiensis* embryos are easy to manipulate via microinjection and thus can be subjected to a number of experiments designed to analyze their development (Gerberding *et al.*, 2002).

Developing *P. hawaiiensis* embryos are optically clear, thus allowing for both detailed microscopic analysis *in situ* and the use of fluorescently tagged molecules (fluorescent dextrans, GFP, or DsRed) in live embryos. The yolk, while opaque, is sequestered early in development to the center of the developing egg and then later to the developing midgut of the embryo. The presence of the colored yolk facilitates identification of embryonic cells during the early stages of development. In addition, early cleavage is holoblastic (total), allowing the fates of individual early cells to be explored through experimental manipulation (Gerberding *et al.*, 2002; Extavour, 2005).

Mating and Fertilization

Sexually mature male and female *P. hawaiiensis* form mating pairs in which the males grasp and hold the smaller females with their second thoracic appendages (T2, gnathopods) until mating occurs. The pairs remain in pre-mating amplexus until the female molts. At this time the male deposits sperm into the females paired oviducts and then releases her. Before the female's new cuticle hardens she sheds her eggs into a ventral brood pouch through two bilaterally symmetric oviducts, fertilizing them in the process. The brood pouch itself is composed of several modified, flattened, and interlacing ventral appendage branches (endites termed oostegites) from the second through the fifth thoracic appendages (T2–T5).

Mature Oocytes

In vivo. Mature oocytes, visible in females through the dorsal thoracic cuticle, are arranged in a row in each of two symmetrical tubes parallel to the A-P axis flanking the midgut. The oocyte nucleus is visible as a whitish oval near the middle of each individual mature oocyte (Fig. 3a). The eggs are fertilized during extrusion through the oviducts located in the posterior ventral region of the fifth thoracic segment (T5).

S1 Stage 1 (0–4 h; 0–1.6%)

One-cell

In vivo. Each ovary releases its eggs in a thinly sheathed transparent sac that expands and disintegrates within ~2 h of egg release. Freshly shed eggs initially adhere to one another and have no distinct morphology. Within the first hour of egg lay the eggs lose their adhesion to one another and the outer chorion shell hardens. Individual eggs, once hardened, are generally elliptical

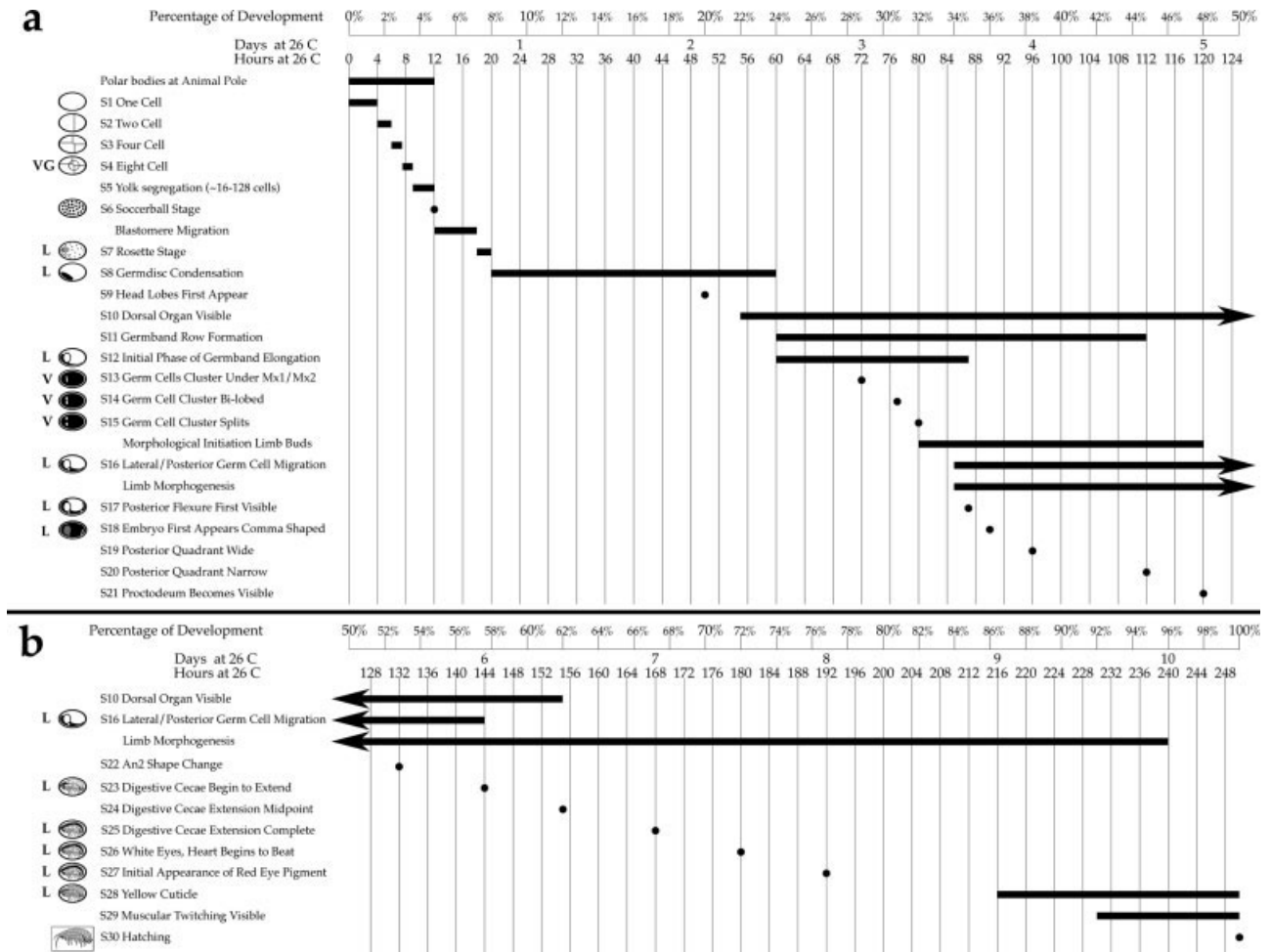


FIG. 2. *P. hawaiiensis* embryogenesis 0–100%. Axis representing percentage of embryonic development and elapsed time in days and hours runs from left to right along the top of panels **a** and **b**. Stage number, stage schematic, and short descriptor run from top to bottom along the left side of panels **a** and **b**. Vegetal view is indicated by VG, lateral view is indicated by L, and ventral view is indicated by V. **a**: Embryonic events and stages from 0–50% of development. Events persisting past 50% of development are marked by arrowheads at far right. **b**: Embryonic events and stages from 50–100% of development. Events beginning earlier than 50% of development are marked by arrowheads at far left.

and tend to have a more rounded end and a more pointed end along the long axis of the egg (Fig. 3b).

The oocyte/egg yolk color ranges between shades of brown, green, gray, and purple. Within a single brood, however, yolk color is uniform and appears to be largely influenced by diet. The yolk granules initially appear homogenous in size and shape.

Fixed + DAPI. While difficult to visualize due to interference from the surrounding opaque yolk, the nucleus appears faintly at approximately the center of the egg. The two polar bodies are visible as brightly stained nuclei at the surface of the egg, and their position was used to determine the early animal and vegetal poles. As in most animals, the polar bodies (animal pole) are associated with the cells that will give rise to the ectoderm and are opposite the mesendodermal cell lineages associated with the vegetal pole (see below for lineage information). Unlike most other animals, however,

the yolk-rich cells are associated with the animal pole of *Parhyale*. The polar bodies remain fixed in position at the animal pole on the egg surface through the third total cell cleavage cycle (S1–S4; Fig. 4a).

S2 Stage 2 (4–6 h; 1.6–2.4%)

Two-cell

In vivo. The first cleavage is total. It is always meridional and perpendicular to the long axis of the egg and thus runs parallel to the animal–vegetal axis. This cleavage is slightly unequal and results in a two-cell embryo (Fig. 3c).

Fixed + DAPI. As with the one-cell embryo, it is difficult to visualize the nuclei of the two-cell embryo due to interference from the surrounding yolk. Initially, the sister nuclei are faintly discernable along the approximate equator of the embryo and do not appear to move far

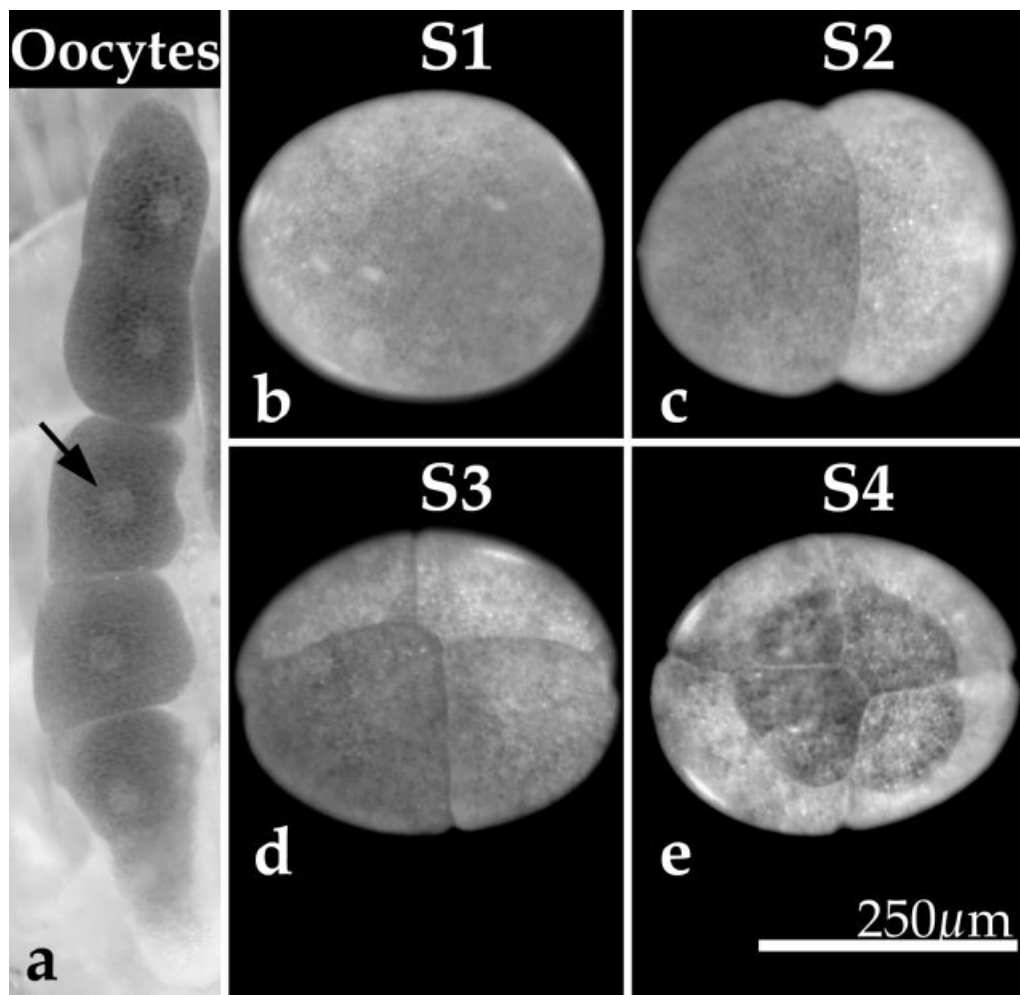


FIG. 3. *P. hawaiiensis* oocytes and Stages 1–4 (S1–S4). **a:** Right ovary with six mature oocytes (anterior up, posterior down). The oocyte nucleus (arrow) is visible as a white oval in the yolk-laden oocyte. **b:** Stage 1 (S1), single uncleaved cell. **c:** Stage 2 (S2), the first cleavage plane is meridional and slightly asymmetric generating a smaller and a larger cell. **d:** Stage 3 (S3), the second cleavage plane is meridional and also slightly asymmetric generating a smaller cell, a larger cell, and two intermediate-sized cells. **e:** Stage 4 (S4), vegetal view, the third cleavage plane is equatorial and highly asymmetric generating an eight cell embryo composed of four macromeres and four micromeres.

from one another. The two nuclei then begin to migrate towards the vegetal pole. The polar bodies continue to be visible as two brightly stained nuclei at the animal pole adjacent to the completed cleavage furrow (Fig. 4a).

S3 Stage 3 (6–7.5 h; 2.4–3.0%)

Four-cell

In vivo. The second cleavage is total. It is always meridional and parallel to both the long axis of the egg and the animal-vegetal axis. This cleavage is slightly unequal and results in a four-cell embryo (Fig. 3d). The second cleavage furrow always initiates at the vegetal pole of the egg and spreads towards the animal pole (Fig. 4a).

Fixed + DAPI. The nuclei at the four-cell stage are clearly visible through the surrounding yolk. The polar bodies remain visible as two bright nuclei at the animal pole adjacent to the two completed cleavage furrows (Fig. 4a,b).

S4 Stage 4 (7.5–9 h; 3.0–3.6%)

Eight-cell

In vivo. Immediately preceding the third cleavage the egg changes shape somewhat and becomes flattened along the animal pole and progressively dome-like along the vegetal pole. The third cleavage is total. It is always perpendicular to the plane of cleavage of both the first and second cleavage, and thus equatorial. This cleavage is always highly unequal. Completion of this cleavage plane establishes a set of four macromeres and four micromeres (Figs. 3e, 4). The four micromeres are cleaved off towards the dome-like vegetal pole.

Each of the eight cells can be uniquely identified based on their relative size and shape and each bears a distinct fate (Gerberding *et al.*, 2002). The four macromere fates are the following: right ectoderm (Er), left ectoderm (El), posterior ectoderm (Ep), and visceral and anterior mesoderm (Mav) (Fig. 4c). In Gerberding *et al.*

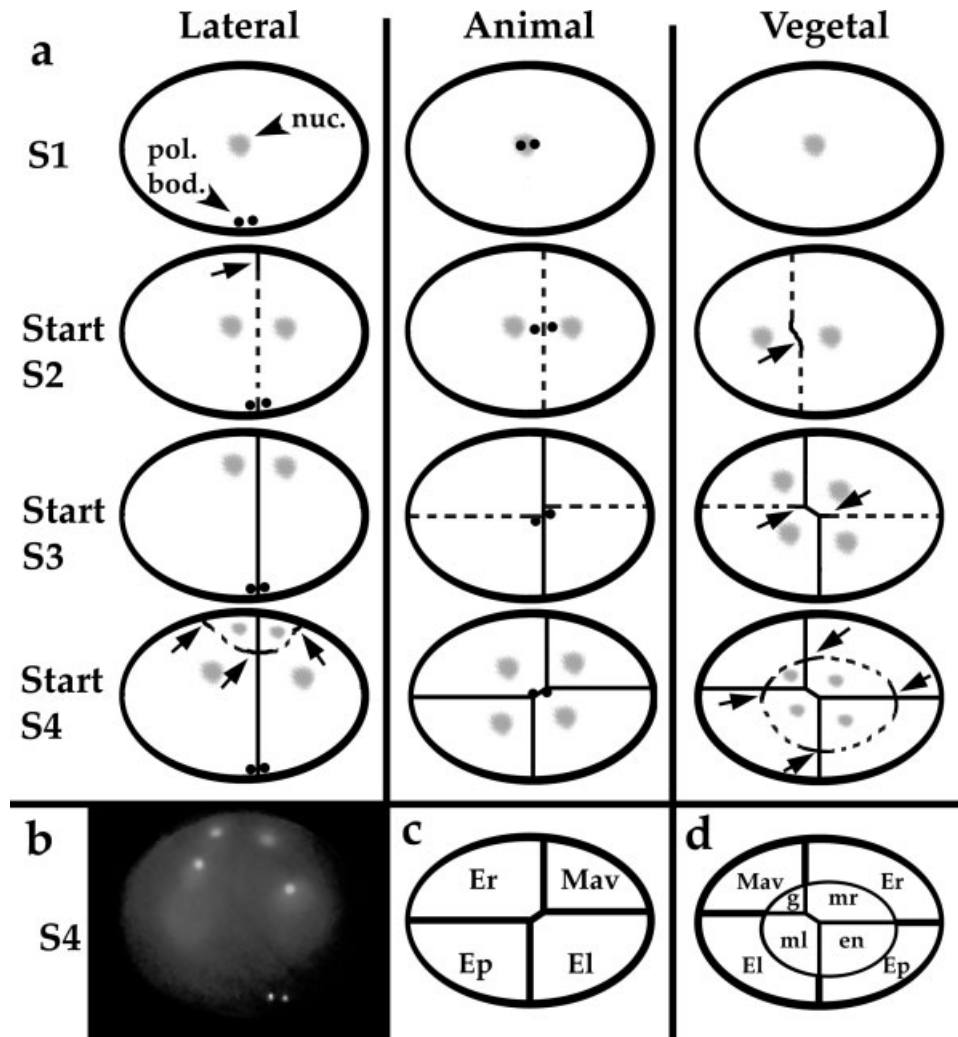


FIG. 4. *P. hawaiiensis* S1–S4 cleavage patterns. **a:** Columns from left to right show lateral, animal, and vegetal views (animal and vegetal views are in mirror image orientation) of S1–S4 embryos. An arrow indicates the initiating position of each cleavage plane (black line), and the position of the completed cleavage plane is indicated by the continuation of a black dashed line. Nuclei are in light gray (arrowhead) and the two polar bodies are represented by two black dots (arrowhead). The position of the polar bodies was used to define the animal–vegetal axis. **b:** A lateral view of an S4 embryo stained with DAPI showing the relative positions of the four nuclei (at the top of the image) and the two polar bodies (at the bottom of the image). Animal (**c**) and vegetal (**d**) schematics indicating fates of the four macromeres and four micromeres. Er, El, and Ep give rise to the anterior right, anterior left, and posterior ectoderm, respectively; Mav gives rise to the visceral mesoderm plus anterior head somatic mesoderm; mr and ml give rise to the right and left somatic trunk mesoderm; g gives rise to the germline; and en gives rise to the endoderm. For further details on the lineage patterns, see Gerberding *et al.* (2002).

(2002) the macromere Mav was called Mv, but our more recent findings show that Mav also produces some anterior somatic mesoderm, hence the name alteration. The four micromere fates are the following: right mesoderm (mr), left mesoderm (ml), germline (g), and endoderm (en) (Fig. 4d).

Fixed + DAPI. The nuclei at the eight-cell stage are clearly visible. As the third cleavage begins the four dividing nuclei move into the vegetal hemisphere of the egg. Once cleavage is complete the nuclei become centrally located within each of the eight newly formed cells. The polar bodies remain visible as two bright nuclei at the animal pole (Fig. 4b).

S5 Stage 5 (9.5–12 h; 3.6–4.8%)

Yolk segregation, 16–128 cells

In vivo. Following the eight-cell stage the developing embryo begins to transition to an asymmetric cleavage program which leads to the segregation of the yolk centrotelothically (towards the interior of the egg). During the next few hours the E macromere lineages (Er, El, Ep) appear to have higher rates of proliferation relative to the other five cell lineages. The partitioning of the yolk towards the center of the embryo correlates with a continuing decrease in the size of nucleated cells and the increased visibility of their associated cytoplasmic islands (see Sholtz and Wolff, 2002, for an example of

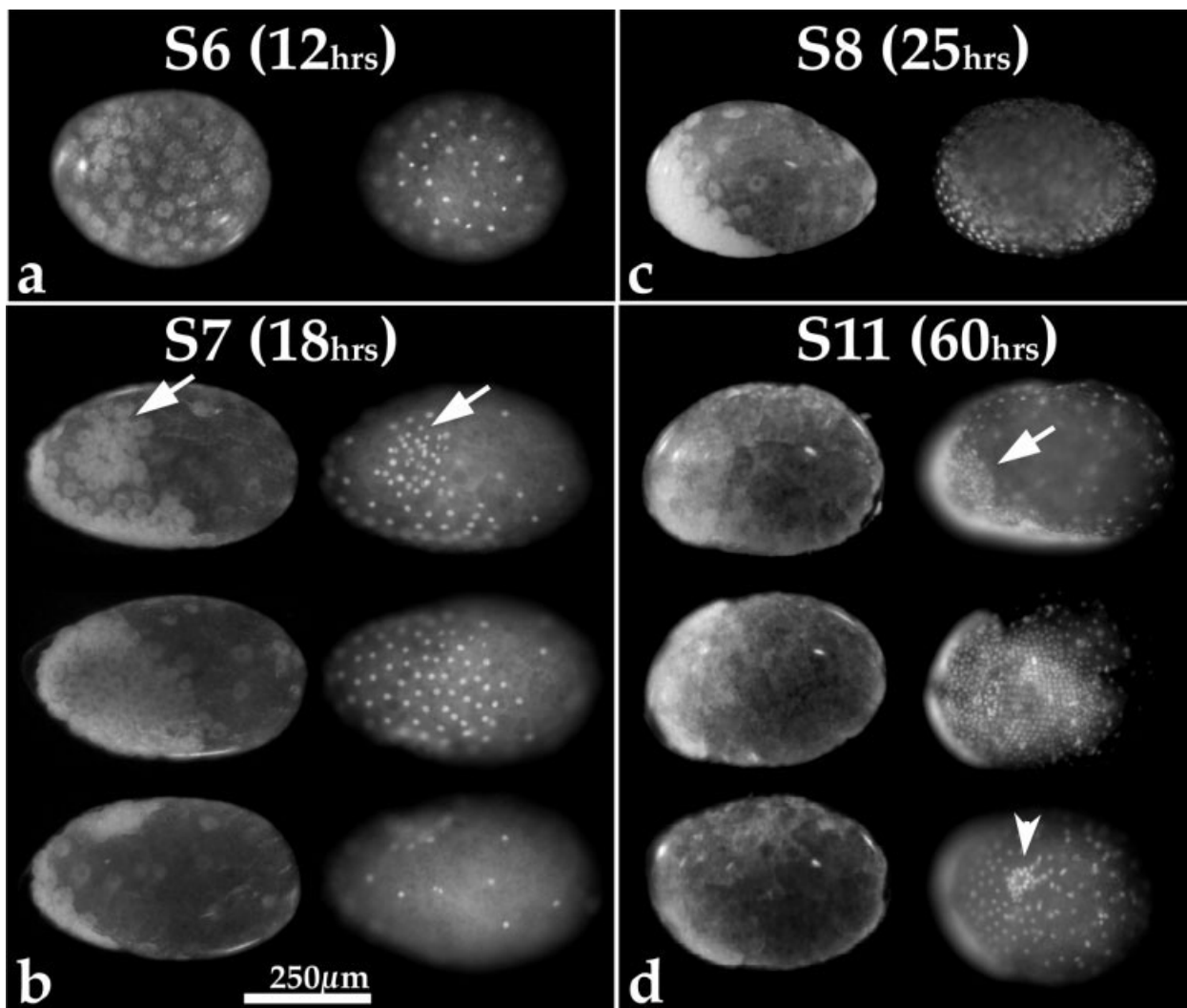


FIG. 5. *P. hawaiiensis* light microscopy and DAPI part I. **a:** Stage 6 (S6), “soccerball” stage; incident light brightfield photo of living embryo (left) and matching DAPI image after fixation (right). Most cells are approximately the same size and evenly distributed around the egg periphery. **b:** Stage 7 (S7), “rosette” stage; same embryo shown at various orientations with brightfield and DAPI staining. Top image pair (lateral view) shows position and distribution of cells and their nuclei in the “rosette.” White arrows indicate the position of rosette cells and nuclei. Middle image pair (animal view) shows the large cluster of cells and nuclei migrating into the position of the future germdisc (there is a slight rotation between brightfield and DAPI images). Bottom image pair (vegetal view) shows the relative lack of cells along the vegetal surface of the embryo as cells migrate towards the future anterior pole of the egg to form the germdisc. **c:** Stage 8 (S8), formation of the germdisc at the anterior end of the egg. Gastrulation and the establishment of multiple germ layers occur as the germdisc is condensing. **d:** Stage 11 (S11), formation of ectodermal cell rows; same embryo shown at various orientations. Top image pair (lateral view) shows the aggregation of cells forming the midgut anlagen (white arrow indicates midgut anlagen nuclei in the DAPI field). Middle image pair (ventral view) shows the organization of the ectoderm into transverse cell rows. Bottom image pair (dorsal view) shows the aggregation of cells forming the dorsal organ (the cluster of nuclei forming the dorsal organ are indicated by the white arrowhead in the DAPI image).

this process in the related amphipod, *Orchestia cavimana*).

Fixed + DAPI. Approximately 2 h after the third cleavage (eight cell, S4) the polar bodies appear to be swallowed by later cleavage furrows and vanish from the embryo exterior.

S6 Stage 6 (12 h; 4.8%)

Soccerball stage

In vivo. At about 12 h of development, all cells of the developing embryo are approaching the same

approximate size due to the accelerated rates of division of macromere progeny. We call this the “soccerball” stage (Fig. 5a). By this stage, most of the yolk appears to have been partitioned centrolecithally towards the center of the developing embryo. The center of the egg is mostly, although not completely, devoid of nuclei at this stage. At the egg surface cell bodies can be clearly seen as whitish cytoplasmic island clusters containing a central and relatively clear hole (the cell nucleus).

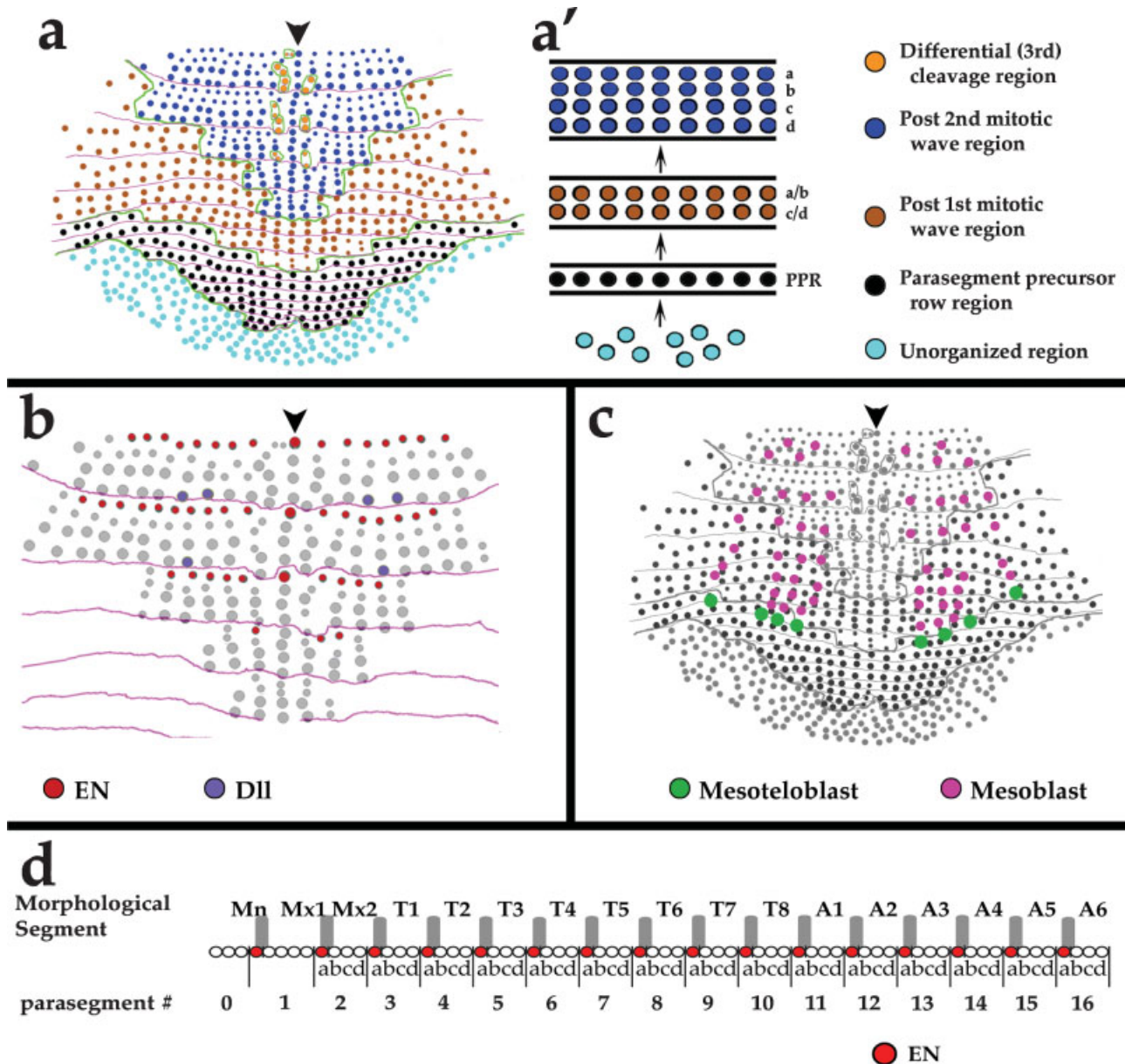


FIG. 6.

Fixed + DAPI. Most of the nuclei are clearly visible and have a fairly even distribution around the egg periphery (Fig. 5a).

S7 Stage 7 (18 h; 7.2%)

Rosette stage

In vivo. After the soccerball stage the first major cell migration events begin and are associated with early gastrulation of the embryo (12–20 h). All visible embryonic cells during this time are largely yolk-free and bear a distinct flattened and sheet-like morphology in which the cytoplasm has an opaque, whitish appearance surrounding a clear nucleus. This morphology is particularly prominent among the actively migrating E1, E2, and E3 macromere descendant cells that form the ectoderm

anlagen. As these cells aggregate towards the presumptive ventral side of the embryo, they begin to form a sheet of cells with regular, tight, and generally hexagonally shaped borders. This migration of cells continues to ~18 h of development (Fig. 5b).

A second distinct cluster of cells, the “rosette,” is also forming at this time by the aggregation of Mav and g descendants. The rosette is distinctly visible at 18 h of development and marks the position of the first group of cells that will move beneath the peripheral surface of the embryo. The rosette marks the future anterior end of the embryonic A-P axis and, once it has migrated under the ectoderm, is the first evidence of multiple germ layers (Fig. 5b).

As most cells continue to condense toward the future anterior pole, a few remain fairly stationary and relatively

widely distributed across the remaining embryo. These cells, however, continue to proliferate and their descendants either migrate into the condensing germdisc or remain stationary outside of the embryo proper (Fig. 5b,c).

Fixed + DAPI. The above cell distributions can be seen very well in DAPI-stained embryos (Fig. 5b). The structure of the rosette is particularly evident in DAPI preparations at this stage and appears as a circular cluster of nuclei that becomes multilayered as the ectoderm anlagen migrates over the stationary rosette cells. At this time the center of the developing egg is still largely devoid of nuclei.

S8 Stage 8 (25 h; 10%)

Germdisc condensation

In vivo. The aggregation of cells, from 20–36 h of development, along the anterior ventral region of the egg comprises the condensing embryonic germdisc. The rosette cells are now positioned under the ectoderm anlagen and begin to actively move to their final positions. A depression in the germdisc can be seen at this time directly overlying the cells of the rosette. This is followed shortly by migration of ml and mr micromere descendants under the ectoderm anlagen regions that flank the rosette. The further development of the germdisc is characterized by continued cell proliferation and a general reduction in cell size. As the germdisc cells become smaller in size they acquire an increasingly whitish, translucent appearance (Fig. 5c).

Fixed + DAPI. At ~25 h of development, DAPI staining reveals a dense aggregation of nuclei along the ventral anterior pole of the developing egg (Fig. 5c). At this time, multiple cell layers are only apparent within the region that will organize to form the embryonic head lobes at the anterior end of the developing embryo.

S9 Stage 9 (50 h; 20%)

Head lobes appear

In vivo. During the next 24 h of development (from 36–60 h of development) the germdisc continues to grow and organize via continued cell proliferation and recruitment of additional cells via migration from both posterior and lateral positions. Within the germdisc there is a continued reduction in cell size and cells take on an epithelial character (compare Fig. 6c,d) and become increasingly organized to form the head lobes and germband of the developing embryo. Cells incorporated into the epithelial sheet exhibit increased adhesion to one another. At this time the relative positions of both the embryonic anterior/posterior axis and dorsal/ventral axis become fixed relative to the egg axis.

Fixed + DAPI. In DAPI preparations, the developing bi-lobed embryonic head is distinctly visible as two symmetrical arcs of cell nuclei with a relatively anuclear v-shaped cleft marking the position of the anterior ventral midline. At this time the germband is just beginning to organize into transverse rows of cells posterior to the arcing head lobes.

S10 Stage 10 (55 h; 22%)

Dorsal organ visible

In vivo. At ~55 h of development the dorsal organ becomes visible as a prominent opaque ring of thickened cells along the anterodorsal midline surface of the developing egg. The dorsal organ remains as a distinctly visible structure late into development (S24, 155 h) and is thought to perform an active osmoregulatory function (Meschenmoser, 1989).

FIG. 6. Schematic of *P. hawaiiensis* germband formation. **a–c:** Anterior is up and the arrowhead indicates ventral midline. **a:** As the germband organizes into parasegments, several discrete regions of mitotic activity and cell organization can be identified. At the posterior end of the germband there is an unorganized region of ectodermal precursor cells (light blue) which become progressively organized into a series of ordered, transverse rows and anterior–posterior columns of cells (black). Each of these transverse rows represents a future parasegment (parasegmental boundaries are indicated by transverse pink lines) and can be assigned a parasegment precursor row number for unambiguous identification. Each parasegment precursor row will then undergo two highly organized rounds of mitotic division. Each round of mitosis begins medially, flanking the midline, and spreads as a wave front laterally, splitting each parasegment precursor row into two cell rows. Cells which have passed through this first round of mitosis are in brown. The second mitotic wave front creates a parasegment composed of four cell rows, and the cells that have reached this point are shown in blue. The third round of mitosis, referred to as a differential division, is not organized in the same regular fashion as the previous two and disrupts the grid. The pattern of division, however, is still stereotypical and can be tracked positionally (shown as orange cells flanking the midline in more anterior regions). **a':** A simplified schematic of the organization and expansion of each parasegment. Unorganized cells (light blue) become arranged into a parasegment precursor row (black). After the first mitotic wave (brown), progeny are identified further as follows: anterior cell row (a/b) and posterior cell row (c/d). After the second mitotic wave (dark blue), cell rows are identified anterior to posterior as: a, b, c, d. **b:** Expression pattern of En (red) and Dll (purple) initiates after each parasegment is composed of four cell rows (parasegment boundaries are indicated by transverse pink lines). En is expressed in the anteriormost parasegmental cell row, a. En expression initiates flanking the midline and spreads laterally. Dll is expressed in the posteriormost parasegmental cell row, d. **c:** The underlying mesoderm is generated progressively from eight mesoteloblasts, indicated in green. The large mesoteloblasts migrate underneath the ectoderm at the same level as the first mitotic wave in the overlying ectoderm, thus they have a slight mediolateral stagger. They divide at regular intervals generating mesoblast progeny, indicated in pink. The mesoblasts organize into rows and align underneath ectodermal cell rows c and d of each parasegment. As with the ectoderm, unique individual mesoteloblast and mesoblast identity can be assigned positionally relative to distance from the midline. Thus, for each parasegment, mesoblast 2 is positioned underneath the first Dll expressing cell of the nascent appendage field (compare panels **b** and **c**). **d:** Numbering system for identification of parasegments and corresponding morphological segments during germband development in malacostracan crustaceans. The parasegment numbering follows the system developed for *Drosophila*. Parasegment precursor rows also correspond to the “Roman numeral rows” found in various malacostracan crustaceans that possess ectoteloblasts (Dohle, 1970, 1976). Development proceeds progressively along the anterior–posterior axis, thus in any given embryo all parasegments are never at the same developmental stage of row formation as shown in this schematic (compare to panels **a** and **b**). Also note that parasegments 0 and 1 do not follow the same pattern with regard to number of cell rows and expression of En as more posterior parasegments, and that parasegment 0 and segment A6 are not shown in their entirety.

Fixed + DAPI. The nuclei forming the dorsal organ are initially visible as a ring, and later as a multilayered oval cluster, along the anterodorsal midline (arrowhead in Fig. 5d).

Segmentation of the Ectoderm and Mesoderm

Within the Amphipoda the entire embryonic ectoderm is patterned from a single sheet of cells that condenses together into a pair of head lobes plus a grid-like array of cells that will form the remainder of the germband. This is in contrast to most other malacostracans, which generate ectodermal segments from posterior T1 on back via a row of ectoteloblast cells (Patel *et al.*, 1989a; Dohle and Scholtz, 1997; Scholtz, 1992). The absence of ectoteloblasts in the amphipod lineage has not, however, substantially altered the way in which the ectodermal sheet is subsequently patterned into segmental units.

Formation of the amphipod germband has been well documented in *Gammarus pulex* (Dohle and Scholtz, 1988, 1997; Scholtz, 1990), *Gammarus roeselii* (Scholtz *et al.*, 1994), and *Orchestia cavimana* (Gerberding and Scholtz, 1999; Scholtz *et al.*, 1993, 1994; Scholtz and Dohle, 1996). The germband of *P. hawaiiensis* exhibits the same mode of development. In *Parhyale*, and other amphipods, the ectoderm precursors arrange into a germband grid that begins anteriorly at the level of the mandibular segment. The formation of the head anterior of the mandibular segment occurs by a different mechanism that is not characterized by the formation of an ectoderm grid. Within the initial ectodermal grid each transverse cell row, as it organizes, represents a developing parasegment. These rows initially undergo two rounds of wave-like, mediolateral, mitotic division to generate four transverse rows of cells (with the exception of parasegments 0 and 1, which do not follow this general pattern, see Fig. 6d and Scholtz *et al.*, 1994). The division of a midline cell lags slightly relative to its left and right neighbors. During each of these two cell division waves the mitotic spindles have a strict A-P orientation. Thus, the resulting daughter cells sort cleanly with respect to row position and transiently generate a parasegment unit composed of four cells rows in the ectoderm (Fig. 6a,a'). Some visible asymmetry with regard to the left and right halves of the developing germband is frequently observed, with cell divisions on the left and right halves slightly out of phase with one another by ~1–2 mitoses.

The naming convention for identification of positions along the A-P axis was initially established by Dohle (1970, 1976). The initial row progeny produced by a round of ectoteloblast division was known as a Roman numeral row. It was subsequently shown that these rows were indeed the precursors to precisely one parasegment unit of the animal (Patel *et al.*, 1989a). Thus, for *Parhyale* each initial transverse cell row can be ascribed a parasegment precursor row designation (Fig. 6a',d). For example, the cells of parasegment precursor row 7 generates the cells which

will make up the posterior compartment of T4 and the anterior compartment of T5 (Fig. 6d; we follow the *Drosophila* convention for starting the numbering of parasegment 1 with the posterior compartment of the mandibular segment). As the first mitotic wave progresses through a transverse parasegment precursor cell row, the progeny generated are an anterior cell row named 7 a/b and a posterior cell row named 7 c/d. During the second mitotic wave, each cell row generates an anterior and posterior progeny cell row thus giving rise to four cell rows; 7a, 7b, 7c, 7d (Fig. 6a',d). To identify lateral positions, the midline is 0 and positions to the left or right are given Arabic numeral identifiers with a left or right distinction (7 d4r = d cell, fourth to the right of the midline, derived from the 7th parasegment precursor cell row). Subsequent ectodermal divisions, while reproducible, occur with a more complicated pattern and timing, and it is at this time that morphological segments are established. The morphological segment boundaries run roughly between "b" row progeny. The contribution of "b" progeny to anterior and posterior segment compartments varies slightly depending on the position along the dorsal-ventral axis being examined.

The segmental mesoderm from T1 and posterior is generated via mesoteloblastic growth as in other crustaceans (Dohle and Scholtz, 1988, 1997; Scholtz, 1990). *Parhyale hawaiiensis* possesses eight mesoteloblasts, four on either side of the midline. These mesoteloblasts go through a highly ordered series of asymmetric divisions to generate progeny called mesoblasts, and as they do so the mesoteloblasts themselves shift posteriorly beneath the developing ectodermal grid. The resulting mesoblasts are organized into rows beneath the posterior compartment of each of the forming parasegments (Fig. 6c) and ultimately go on to produce the somatic mesodermal derivatives of the associated segment. Progression of mesoteloblast division and migration is correlated with the first mitotic wave in developing parasegments of the overlying ectoderm. As the first mitotic wave progresses mediolaterally in the ectoderm, mesoteloblasts divide and migrate with the leading edge of the mitotic waves (Fig. 6c). This results in the mesoteloblasts having both a well-defined mediolateral, as well as A-P, stagger. Mesoteloblasts are named according to their relationship to the midline and left or right side of the embryo. Thus, from right to left the mesoteloblasts are Mr4, Mr3, Mr2, Mr1, MI1, MI2, MI3, MI4 (Fig. 6c). The progeny mesoblast cells are named according to their relationship with the overlying ectoderm and position relative to the ventral midline. Thus, the most medial mesoblast on the left side of parasegment 8 would be ml1.vi. (Fig. 6c).

Gene Expression

The broadly crossreactive and widely available antibodies to Engrailed (En; Patel *et al.*, 1989a,b) and Dis-

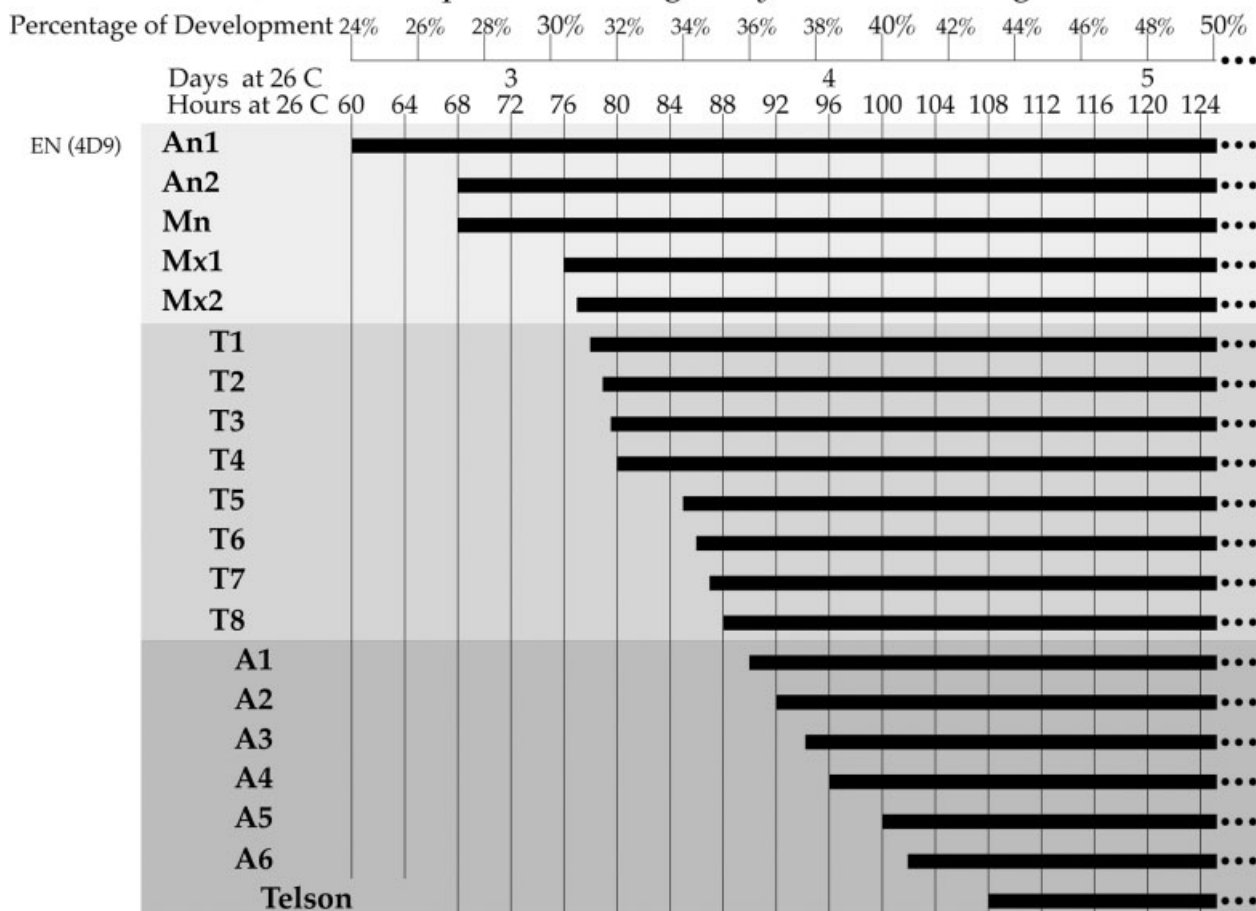
Onset of *ENGRAILED* expression during *Parhyale hawaiensis* segmentation

FIG. 7. Onset of Engrailed expression during *P. hawaiensis* segmentation. Axis representing percentage of embryonic development and elapsed time in days and hours runs left to right along top of the table. Segments are listed along the left side of the table, anterior at top posterior at bottom. Onset of the detection of En protein with MAb 4D9 is marked by black bars. The anterior-posterior pattern of row formation and segmentation is clearly seen from this pattern of Engrailed expression.

tallest (DII; Panganiban *et al.*, 1997) reveal gene expression patterns that are also useful for embryo staging. The initial expression of both En and DII are very closely tied to the pattern of mitosis during the proliferation and development of the germband.

We have followed the expression of En during the initial phases of segmentation (Figs. 7, 8), as well as later embryonic expression within neuroblasts, ganglion mother cells, and specific neurons of the developing CNS (Duman-Scheel and Patel, 1999) (Fig. 9). In *P. hawaiensis*, just as in all other malacostracan crustaceans described so far, En is detected in the anterior cell row of developing parasegments and accumulates in the posterior compartment of morphological segments and appendages (Figs. 6d, 7, 8, 10, 11). The onset of segmental Engrailed expression is shown in Figure 7. Posterior to Mx1 the initial expression of En is in cell row "a" and is always temporally 1–2 cells behind the second mitotic wave front. Later, En is found in a number of neuroblasts and some of their ganglion mother cell progeny (Fig. 9a,b). As neurons in the CNS differentiate, En is expressed in several neurons, includ-

ing the homologs of the IC, LE, ECa, and ECp neurons (Figs. 8g, 9c,d), as well as MNB progeny (Figs. 8f,g, 9c).

DII expression allows us to monitor the initiation and elaboration of appendage patterning. In various arthropod taxa it has been suggested that DII expression differentiates between cells fated to become proximal coxopodite elements (DII negative) from cells fated to become distal telopodite elements (DII positive) (Gonzalez-Crespo and Morata, 1996). In *Parhyale* the expression of DII always initiates in the fourth d cell (d4) lateral of the midline (0) directly overlying the second mesotoloblast cell (ml2/mr2) (Fig. 6b). Temporally, DII initiation occurs when the ectoderm of that parasegment has undergone 1–2 additional asymmetric cleavages in cells flanking the midline (Fig. 6a). Specific events are noted below and can be used for more detailed staging.

S11

En stripe 1 at 60 h

The first En stripe, as detected with the monoclonal antibody 4D9, is visible at 60 h of development and marks

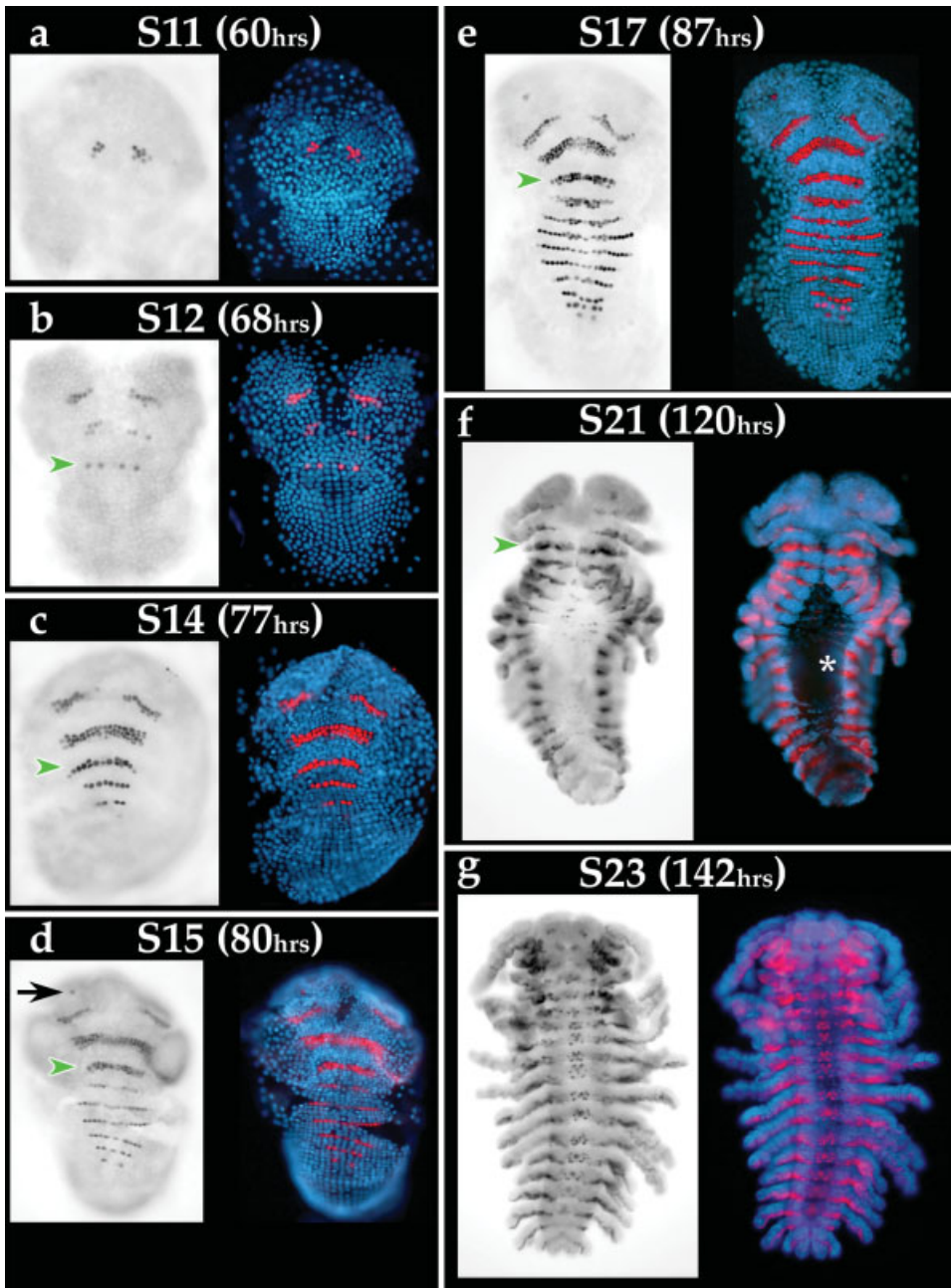


FIG. 8. Engrailed expression in *P. hawaiiensis*. All embryos are oriented anterior up. Brightfield images are to the left and DAPI images are to the right. Anti-En staining (with MAb 4D9) is black in brightfield images and false-colored red in overlaid DAPI images. The green arrowhead marks the position of the mandibular (Mn) segment En stripe. **a:** Stage 11 (S11), the first expression of En initiates in An1. **b:** Stage 12 (S12) An1, An2, and Mn segments are En-positive. **c:** Stage 14 (S14), five stripes of En are present, with the fifth stripe corresponding to the second maxillae segment (Mx2). **d:** Stage 15 (S15), nine stripes of En are present, as well as the ocular spots anterior of the An1 segment (indicated by black arrow). The ninth stripe corresponds with T4. **e:** Stage 17 (S17), 12 stripes of En are present. The twelfth stripe corresponds to T7. **f:** Stage 21 (S21), all segments are En-positive. The white asterisk in the DAPI view indicates the prominent and transient ventral midline split. En-positive MNB progeny are visible lying alternately to the left and to the right of the apparent ventral midline. **g:** Stage 23 (S23), the ventral midline cleft has closed and all segments possess a subset of En positive neurons.

the first antennal segment, An1 (Fig. 8a). For An1, En appears laterally as a single row of cells and expands to approximately two cells wide. Expression of En in the first antennal stripe never crosses the embryonic midline.

Dll expression at 60 h

The first detectable Dll expression is along the anterior region of the developing *Parhyale* head lobes. This expression is anterior and lateral of the first antennal segment (Fig. 10a).

S12

En stripe 2 and 3 at 66–68 h

Either the An2 stripe or the Mn stripe can be the second stripe of En to appear (ratio between two patterns

appears to be 50/50). The An2 stripe initiates laterally as two widely spaced, separate, left–right domains of expression and begins spreading as a two-cell wide (A/P width) domain. The Mn stripe initiates medially as a single row of En expressing cells and spreads laterally (Fig. 8b).

Dll expression 68 h

Shortly after the An2 En domains fuse and the Mn domain has spread to its lateralmost limits, Dll initiates in the An1, An2, and Mn segments.

S14

En stripe 5 at 77 h

By 77 h the developing germband has five stripes of En (En stripe 5 corresponds to the Mx2 segment). For all

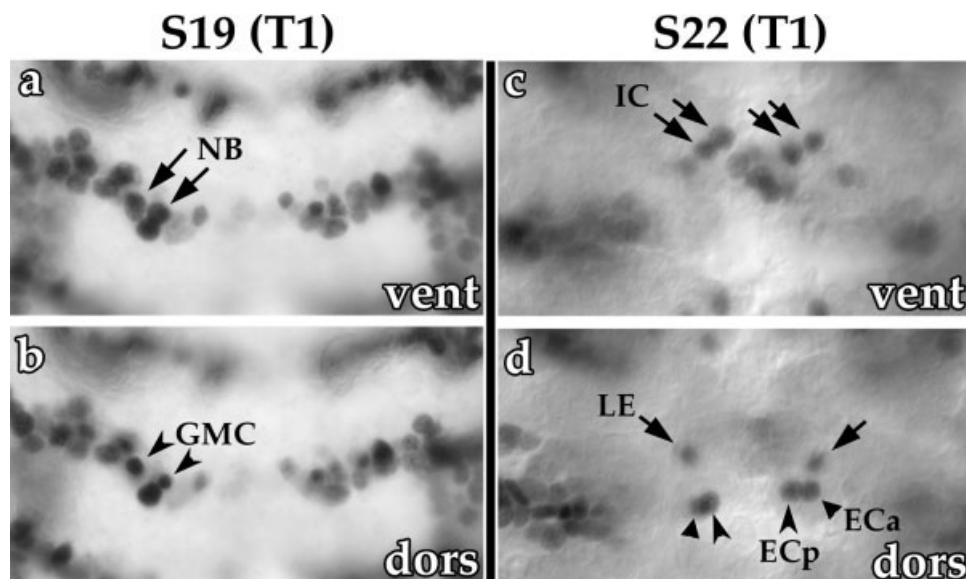


FIG. 9. Identification of Engrailed-positive CNS cells in T1. In all panels anterior is up. **a,b:** Stage 19 (S19). At ~96 h the T1 segment has generated a series of En-positive neuroblasts (NBs) and ganglion mother cells (GMCs). **a:** Ventralmost focal plane shows several En-positive neuroblasts (arrows). **b:** Slightly more dorsal focal plane from embryo shown in **a**. The black arrowheads in **b** indicate the position of the smaller En-positive GMCs directly above the parent NBs shown by arrows in **a**. **c,d:** Stage 23 (S22). At ~140 h T1 has generated a number of positionally identifiable En positive neurons in the CNS. **c:** Ventralmost focal plane of En-positive staining. Black arrows indicate IC neurons. The medial cluster of En-positive cells are presumably MNB progeny cells. **d:** Slightly more dorsal focal plane from embryo shown in **c**. At the level of the connective and commissural axon tracts, black arrows indicate En-positive LE neurons, triangles indicate En-positive ECa neurons, and arrowheads indicate En-positive ECp neurons.

segments that will be incorporated into the cephalon (T1 and anterior), the lateral extent of the En stripe is contiguous with the edge of the developing appendage bud. However, for segmental En domains including T2 and posterior, the En stripe continues laterally and, ultimately, dorsally along the future body wall. En stripe 2 (An2) spreads both medially and laterally and expands to 3–4 cell widths (A/P) after the two separate domains connect along the midline. All En stripes posterior of the mandibular segment arise in a strictly A-P temporal progression (Fig. 7).

Dll at 77 h

By the time the fifth En stripe appears Dll is detectable in An1, An2, and the Mn segments. These Dll domains arise as bilaterally symmetric clusters of cells in which the posterior half of each Dll domain lies within the En-expressing domain and the anterior half of each Dll domain lies just anterior to the En expression domain (e.g., Fig. 10b). Dll protein is detected strongly throughout the developing Mn appendage fields during and after the initial formation of the proximal–distal (P-D) axis. This is in contrast to the insect Mn, in which ectodermal Dll expression is not seen during development of the Mn appendage.

S15

En stripe 9 plus ocular spots at 80 h

The developing germband has nine stripes of En, as well as the bilateral ocular En domains in the developing head (Fig. 8d).

Dll at 80 h

The Mx1 Dll domain lies more medial than any of the other Dll domains and also enlarges at a slower rate than the other Dll domains. All Dll domains from Mx2 posterior initiate in the same way—Dll protein begins to accumulate in cell d4 as the posteriorly abutting cells a4, a5, and then a6 accumulate En protein. After Dll expression begins in d4, the next cell to begin to express Dll is d5 (Fig. 6b). Dll is detected strongly in the labrum, anterior and medial of the An1 domain (Fig. 10b).

S19

En in the CNS at 96 h

The first thoracic segment, T1, has a number of En-positive neuroblasts as well as En-positive GMCs (Fig. 9a,b).

Dll at 96 h

The labral Dll domain is medial and slightly anterior of the En and Dll ocular expression domains. Initiation and early development of the labrum occurs in the preantennal segment (Fig. 10b–d).

S21

En staining in all segments

At 117 h (slightly before S21), En expression is seen in all segments. A subset of the MNB daughter cells are En positive and lie to the right and the left of the midline along the ventral thoracic cleft (Fig. 8f).

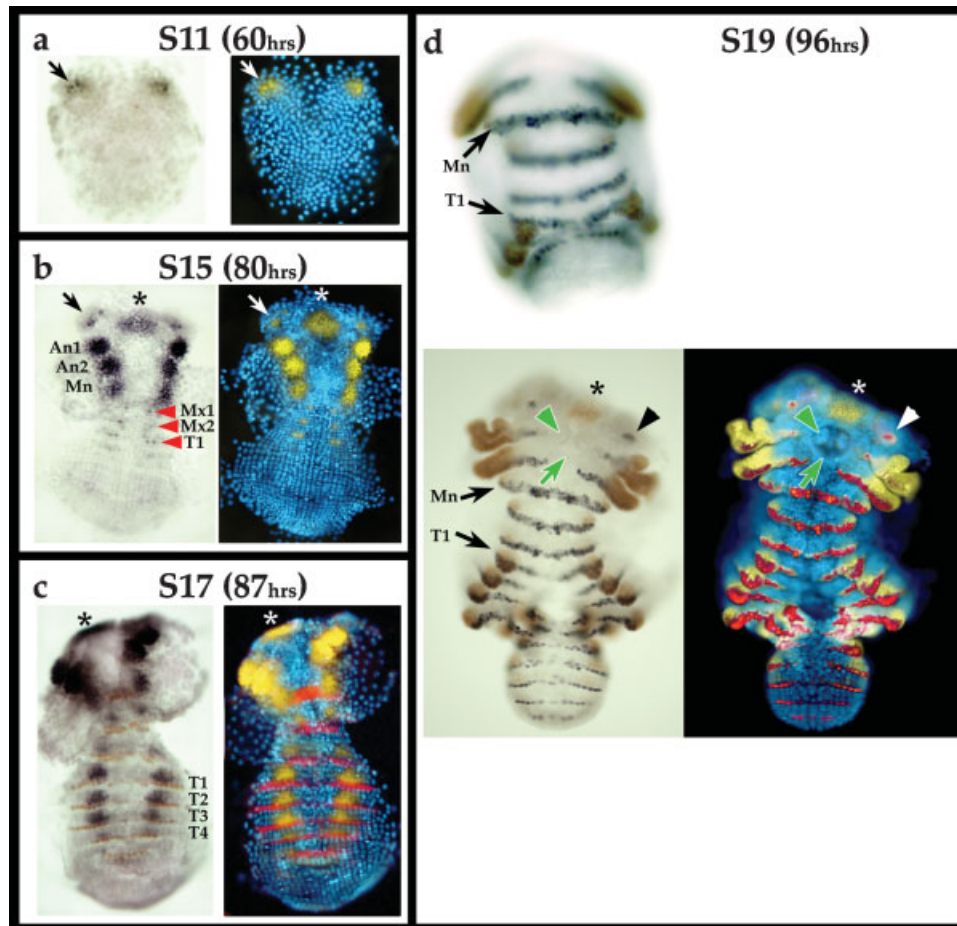


FIG. 10. Distalless and Engrailed Expression in *P. hawaiiensis*. All embryos are oriented anterior up. For each panel brightfield image is on the left and DAPI image is on the right. In **a–c** brightfield images, Dll is in black and En is in brown. In panel **d** brightfield image, Dll is in brown and En is in black. In DAPI images of panels **a–d** Dll is false-colored yellow. In **c,d** DAPI images, En is false-colored red. Because of the manner in which the channel overlay was done in **d**, red indicates either En or En+Dll. **a:** Stage 11 (S11), 60-h germband. Dll initiates in two arcs in the optic lobes anterior of the An1 segment (arrow). En is just beginning to be expressed in the An1 segment and can be seen as a single brown cell on the left side of the brightfield embryo. The DAPI field shows the Mn segment just beginning to organize into transverse cell rows. **b:** Stage 15 (S15), 80-h germband labeled for Dll only. The optic lobes remain Dll-positive (arrow). The medial labrum is beginning to express Dll anterior of the An1 appendage field (asterisk). The An1, An2, and Mn appendage fields are Dll-positive. The Mx1, Mx2, and T1 appendage fields are just beginning to initiate Dll expression (red arrowheads). **c:** Stage 17 (S17), 87-h germband. En has just initiated expression in T6 (out of focal plane). Dll has just initiated expression in the T5 appendage field. Dll expression in Mx1 and Mx2 appendage fields remains at low levels. The Mn is still expressing Dll broadly throughout. The asterisk marks Dll expression in the developing labrum anterior of An1. **d:** Stage 19 (S19), 96-h embryo. Upper image shows embryo before it was dissected flat. En has initiated in A4 and is visible in the posterior compartment of developing antennal, gnathal, and thoracic appendage fields. The transient midline cleft has begun to form in the posterior thoracic region. The forming stomodeum is clearly visible and is positioned medial of An1 (green arrow). Lateral esophageal projections are visible forming at the interior lateral edges of the stomodeum (green arrowhead). Neither of these structures (stomodeum nor lateral esophageal projections) are Dll- or En-positive. The Dll-positive labrum is visible just anterior of the developing stomodeum (asterisk). The En-positive staining in the developing optic lobes remains visible (black arrowhead in brightfield image, white arrowhead in DAPI image).

S22

En staining is widely present in the developing embryonic CNS at 139 h (Fig. 9c,d)

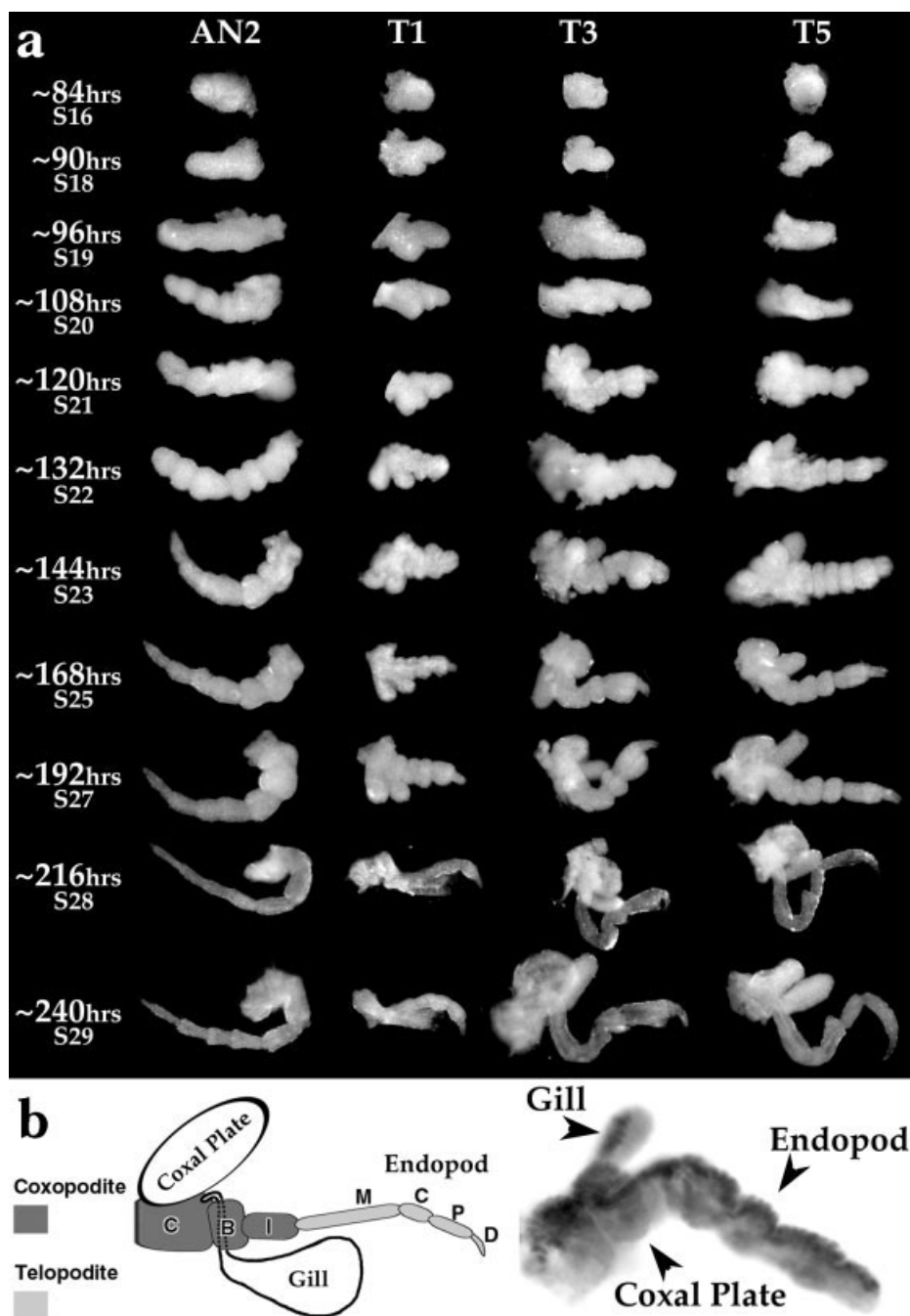
The thoracic ventral midline split has closed. The T1 segment is positive for a number of identifiable neurons: ECa, ECp, LE, and IC (Figs. 8g, 9c,d) (Duman-Scheel and Patel, 1999).

S24

En staining persists

En expression remains in the posterior compartment of developing segments and dorsal body wall as well as in the developing CNS. The expression pattern remains fairly static until cuticle deposition (S28, at 216 h) precludes detection via standard antibody-based histochemical protocols.

FIG. 11. *P. hawaiiensis* appendage development. **a:** Photos of An2, T1, T3, and T5 appendages from 84–240 h of development. All appendages are from the left side of the animal. **b:** An amphipod pereopod schematic is on the left. Dark gray shading indicates the basal elements forming the coxopodite; coxa (C), basis (B), and ischium (I). Light gray shading indicates the distal elements forming the telopodite; merus (M), carpus (C), propodus (P), and dactyl (D). Two dorsal branches initiate from the pereopod coxa. The outer branch is the coxal plate. The inner, epipod, branch initiates at the distal posterior region of the coxa from which it articulates both posteriorly and medially. It forms a laterally flattened and highly vascularized sheet that can perform respiratory functions (gill). To the right is pereopod T5 stained with En (marking the posterior compartment) in black. The appendage is oriented dorsal up. The wide flat dorsal branch initiating across the coxa is the coxal plate. The dorsal branch initiating from the posterior distal margin is the gill. The gill is a modified epipod.



S11 Stage 11 (60 h; 24%)

Formation of the germband: initial ectodermal and mesodermal cell rows form

Engrailed expression: An1

In vivo. Progressive formation of ectodermal and mesodermal cell rows along the A-P axis begins at 60 h of development and continues to S21 (120 h of development). Also at this time, the midgut anlagen are becoming visible as lateral disc-like structures flanking and just posterior of the head lobes (Fig. 5d).

Fixed + DAPI. At 60 h of development the organization of the ectoderm into grid-like rows and columns is especially striking in DAPI-stained preparations (Figs. 5d, 8a, 10a). Several “numeral rows” (parasegment precursor rows) have organized by this time, with the anterior-most transverse row forming parasegment 1. The first mediolateral mitotic wave (forming the a/b and c/d progeny) has not yet begun. After the formation of the first two anterior transverse rows, cells forming the embryonic ventral midline begin to organize into a single A-P column. As development proceeds, additional organized

“numeral” rows will form in an anterior to posterior progression. Also at this stage, the nuclei defining the ring shaped walls of the midgut anlagen discs are well defined and appear relatively closely packed (Fig. 5d).

S12 Stage 12 (68 h; 27.2%)

Initial germband elongation stage

Engrailed expression: An1, An2, Mn

In vivo. The bi-lobed head is multilayered at this time and appears as a distinct clearing at the anterior ventral end of the egg. The laterally positioned midgut anlagen have become very prominent disc-shaped structures. The dorsal organ is clearly visible as a thick ring and lies along the dorsal anterior midline of the developing embryo. The region of the germband from Mx1 and posterior appears as a relatively optically clear region ventral and posterior of the developing head segments and gut anlagen.

Fixed + DAPI. In DAPI-stained embryos the germband region of the embryo has the highest density of nuclei and the ectoderm posterior to the Mn is clearly organized into mediolateral columns and A-P rows. At 68 h of development the first mediolateral mitotic wave can be found moving across parasegment precursor row 3 (Fig. 8b). Nuclei found within the disc-shaped gut anlagen appear to be dispersed and occur in several layers; however, the nuclei positioned along the edges of the discs appear to be more closely arranged. The ectodermal cells of the anterior head segments have begun to undergo asymmetric cleavages, and at least some of the progeny cells are likely to be neuroblasts (e.g., Fig. 6a).

Appendage Development

For the purposes of providing additional staging criteria, we have chosen to describe the development of four appendages, the second antenna (An2), the first thoracic appendage (maxilliped; T1), the third thoracic appendage (gnathopod; T3), and the fifth thoracic appendage (pereopod; T5) in some detail. The appendages were dissected intact from developing embryos to facilitate description. Each of the four appendages bears a distinct morphology and thus brief descriptions at various time points can provide landmarks to easily gauge the relative age of the embryo under examination (Fig. 11).

The antennae are uniquely derived appendages. The five proximal-most elements of An2 comprise the peduncle and each individual element is rather stout in appearance. The remaining distal elements are termed flagella and they progressively narrow along the P-D axis of An2. The maxilliped on T1 is strongly modified to serve as the outermost feeding appendage of the buccal mass (posteriormost feeding appendage along the A-P axis, see Fig. 1). The maxilliped possesses two ventral limb branches (endites). The T3 gnathopod and T5 pereopod appendages serve grasping and locomotory functions, respectively. Both T3 and T5 possess a coxal plate and a modified epipod. The P-D axis of the

endopod (the primary appendage branch) of T1, T3, and T5 is composed of the coxa, basis, ischium, merus, carpus, propodus, and dactyl elements (Fig. 11).

S13 Stage 13 (72 h; 28.8%)

Germ cell cluster visible

Engrailed expression: An1, An2, Mn

In vivo. Bilateral germ cell cluster migration: During the development of the embryonic germband the germ cells become clearly visible underneath the developing maxillae 1 (Mx1) and maxillae 2 (Mx2) segments. Initially, they are present as a single medial cluster of whitish cells underneath the ectoderm at ~72 h of development. A similar position of the germ cells during germband development in a related amphipod, *Gammarus pulex*, was described by Weygoldt (1958) based on fixed material. Additional descriptions of germ cell development in *Parhyale* can be found in Gerberding *et al.* (2002) and Extavour (2005).

Appendage buds begin to visibly project from the ventral ectodermal surface in an anterior-to-posterior progression at 72 h of development beginning with the first antennae (An1).

Fixed + DAPI. In DAPI preparations the progression of appendage development can be clearly tracked by the appearance of dense aggregations of nuclei along the P-D axis of each appendage. The An1 and An2 appendages are beginning to extend along their respective P-D axes.

S14 Stage 14 (77 h; 30.8%)

Germ cell cluster bi-lobed

Engrailed expression: An1, An2, Mn, Mx1, Mx2

In vivo. At 77 h of development the ventral germband has expanded posteriorly the full length of the egg. The bilateral midgut anlagen have become two well-defined circular structures flanking the gnathal segments (Fig. 12a). The germ cells are beginning to separate into two bilaterally opposed whitish clusters. The anterior cephalon continues to thicken and is becoming optically clear (Fig. 12a).

Fixed + DAPI. In DAPI-stained embryos the ectoderm grid is clearly visible and extends the full length of the ventral surface of the egg. Nuclei associated with the midgut anlagen occur in several layers (Fig. 12a). Differential and asymmetric cleavages begin to spread throughout the ectodermal grid (Fig. 12a; for further information about differential cleavages, see section on ectoderm and mesoderm segmentation). Some of the progeny of these differential, asymmetric cleavages are likely to be neuronal stem cells (neuroblasts) by both cell position and cell cleavage criterion (Dohle, 1976; Scholtz, 1990, 1992).

S15 Stage 15 (80 h; 32%)

Germ cell cluster splits

Engrailed expression: Ocular spots, An1, An2, Mn, Mx1, Mx2, T1, T2, T3, T4

In vivo. The cluster of germ cells located ventromedially between segments Mx1 and Mx2 has completely split into two bilaterally opposed whitish clusters that

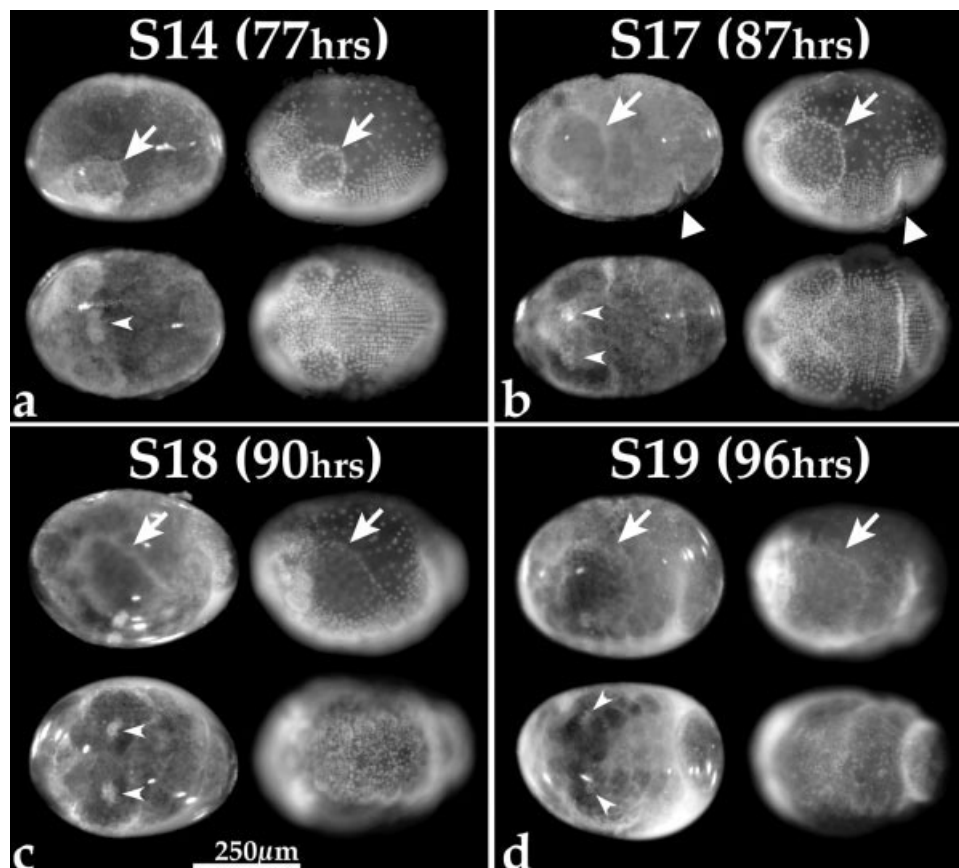


FIG. 12. *P. hawaiiensis* light microscopy and DAPI part II. Live brightfield and matching postfixation DAPI images showing lateral (upper image pairs) and ventral (lower image pairs) views. **a:** Stage 14 (S14), the white arrow on the lateral view (upper image pair), shows the ovoid shaped midgut anlagen. The white arrowhead at the midline on ventral view (lower image), shows the position of the germ cell clusters as they are separating from one another. Organization of the ectoderm into transverse cell rows ventrally is clearly visible in the DAPI view. **b:** Stage 17 (S17), ventral flexure visible. White triangles on the lateral view (upper), indicates the position at which the posterior ventral flexure initiates (T4/T5). White arrow shows the position of the midgut anlagen. White arrowheads flanking the midline on the ventral view (lower), show the position of the migrating germ cell clusters. The ventral flexure is clearly visible in the DAPI images. **c:** Stage 18 (S18). White arrow on lateral view (upper) shows the position of the midgut anlagen. The posterior, ventral edge of the anlagen is coincident with T2. The deepening ventral flexure is clearly visible in the posterior quadrant of the egg. White arrowheads on ventral view (lower) show the position of the migrating germ cell clusters. The ventral DAPI field shows the formation of appendage fields along the embryo. **d:** Stage 19 (S19), paddle-shaped posterior quadrant. White arrow on lateral view (upper) shows the position of the ovoid shaped midgut anlagen. The posterior region of the embryo has expanded laterally and posteriorly forming a paddle shaped posterior quadrant. White arrowheads on ventral view (lower) show the position of the migrating germ cell clusters just lateral of the Mx1 and Mx2 appendage fields.

flank the embryonic midline. Each cluster of germ cells then begins to move laterally away from the embryonic midline. The An1, An2, and Mn appendages are clearly visible as proximal distal outgrowths from the developing embryonic head.

S16 Stage 16 (85 h; 34%)

Bilateral germ cell cluster migration

Engrailed expression: Ocular spots, An1, An2, Mn, Mx1, Mx2, T1, T2, T3, T4, T5, T6

In vivo. The two germ cell clusters have begun to migrate laterally and posteriorly. This migration is visible from Stage 16 to Stage 23 (Figs. 12, 13).

Fixed + DAPI. The An2 appendage primordium has begun to elongate and is clearly composed of two P-D

elements. The T1 appendage primordium has begun to elongate and is composed of a single element. The T3 and T5 appendage primordia are visible as buds (Fig. 11a).

S17 Stage 17 (87 h; 34.8%)

Posterior (ventral) flexure visible

Engrailed expression: Ocular spots, An1, An2, Mn, Mx1, Mx2, T1, T2, T3, T4, T5, T6, T7

In vivo. As the germband elongates it begins to fold inwards toward the egg interior at segment T5 (Fig. 12b). As elongation proceeds, this posterior (ventral) flexure expands to include more anterior and more posterior segments. This flexure is visible as a clear furrow in the germband when viewed from the side (Figs. 12, 13).

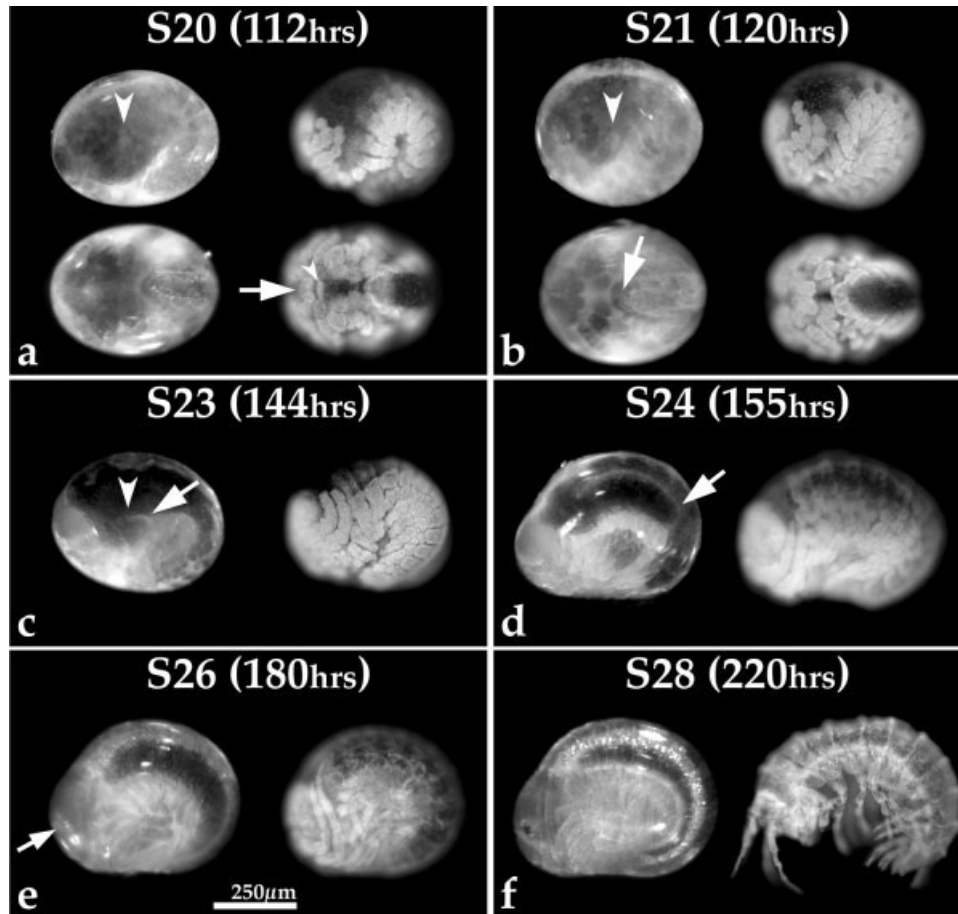


FIG. 13. *P. hawaiiensis* light microscopy and DAPI part III. Live brightfield and matching postfixation DAPI images showing lateral (upper image pairs) and ventral (lower image pairs) views in **a** and **b** and just lateral views in **c–f**. **a:** Stage 20 (S20), posterior quadrant narrows, the second mitotic wave has passed through all parasegments of the ectoderm, and the telson appears. Larger white arrowhead on lateral view (upper) shows position of the migrating germ cell clusters. The posterior quadrant has significantly narrowed. A wide area of clearing is visible dorsally. The highest concentration of nuclei is in the developing appendages and cephalon. In lower, ventral view, the telson is apparent and projects forward to T1. The labrum (white arrow) is visible medially projecting posterior towards the stomodeum from between the antennal segments. The lower edge of the stomodeum (smaller white arrowhead) is visible medially and just posterior of the labrum. Just posterior of the developing stomodeum, the paragnaths can be seen projecting medially from the ventral base of the mandibles. **b:** Stage 21 (S21) hindgut proctodeum becomes visible. White arrowhead on lateral view (upper) shows position of the germ cell clusters. In ventral view (lower) the hindgut proctodeum (white arrow) is visible as a wedge-shaped ridge of cells at the posterior end of the embryo. The labrum has extended significantly. Just posterior and ventral of the labrum are the prominent mandibles that are flanked medially by the paragnaths. **c:** Stage 23 (S23), digestive caecae begins to extend. The white arrow indicates the initial posterior projection of the digestive caecum. The white arrowhead shows the position of the germ cell clusters at the shoulder of the digestive caecae. The germ cells will come to occupy a position on the medial surface of the extending caecae, facing the midgut. DAPI staining clearly shows body wall segmental boundaries extending dorsally. **d:** Stage 24 (S24), midpoint of digestive caecae extension. The white arrow shows the posterior extent of extending caecum (~T7). Yolk granules have cleared from the cephalon. Body tergites and coxal plates are visible. **e:** Stage 26 (S26), white-eyes and beating heart. The white arrow indicates the position of the developing rhabdomeres. The embryo is beginning to visibly accumulate cuticle, and the appendages are achieving their final hatching morphology. **f:** Stage 28 (S28), yellow cuticle. As cuticle continues to accumulate the embryo acquires a yellow-gold appearance. The eye rhabdomeres fields appear intensely red, the limbs have acquired their final morphology, and the digestive caecae are significantly depleted of yolk stores.

Fixed + DAPI. In DAPI preparations at 87 h the developing ventral surface has the highest density of nuclei and is organized into clear segmental units (Fig. 12b). In comparison, the dorsal and lateral surfaces of the developing embryo have relatively sparse cell populations and temporally lag behind in terms of segmental organization (Fig. 12b). The midgut anlagen have increased in size dramatically and meet one another at their ventralmost margin and begin to fuse (Fig. 12b). The two germ clusters

are clearly visible sandwiched between the ectoderm and the midgut anlagen (arrowheads, Fig. 12b).

S18 Stage 18 (90 h; 36%)

Ventral flexure of embryo

Engrailed expression: Ocular spots, An1, An2, Mn, Mx1, Mx2, T1, T2, T3, T4, T5, T6, T7, T8, A1

In vivo. At 90 h ventral flexure of the embryo is apparent (Fig. 12c). The infolded region includes the entire

ventral region of the abdomen and a large part of the posterior thoracic region. The An1, An2, and Mn segments are beginning to expand dorsally (Fig. 12c). Ventrally, the germ cell clusters have migrated to positions just lateral of the Mx1 and Mx2 appendage fields and appear as two gray-white masses (Fig. 12c).

Fixed + DAPI. Dorsally, nuclei still appear rather dispersed and unorganized, with the notable exception of the anterior dorsal surface where the dorsal organ is located and the posterior dorsal surface of the egg where a portion of the posterior end of the embryo is now visible. At the dorsal organ, nuclei are arranged in a ring. The nuclei of the midgut anlagen are visible as two medially fused, rhomboid-shaped aggregations with the posterior ventral margin projecting to T2 (Fig. 12c). Ventrally, nuclei are dense and clearly ordered into segmental units along the A-P axis of the embryo. Ventral nuclei are particularly dense in the developing appendage buds of An1, An2, Mn, Mx1, Mx2, T1, and T2 (Fig. 12c).

The length of the An2 second element has increased relative to the proximal first element. The T1 appendage is composed of two elements of which the proximal element begins to bulge medially. The T3 and T5 appendages have begun to elongate (Fig. 11a).

S19 Stage 19 (96 h; 38.4%)

Posterior widens

Engrailed expression: Ocular spots, An1, An2, Mn, Mx1, Mx2, T1, T2, T3, T4, T5, T6, T7, T8, A1, A2, A3, A4

In vivo. At 96 h the region enclosed by posterior flexure has broadened laterally, extended posteriorly, and appears paddle-shaped (Fig. 12d). The germ cells have maintained their position lateral to Mx1 and Mx2 appendages; however, they have become slightly more opaque in appearance. The head region has moved dorsally to occupy the anterior face of the egg. The midgut anlagen have increased in size and appear to be ovoid. Cells across the face of the midgut anlagen are large and clearly organized into a hexagonal array (Fig. 12d).

Fixed + DAPI. The extreme dorsal region of the embryo still bears relatively few nuclei, but the lateral thoracic ectoderm now shows organization of nuclei into rows. The posterior paddle retains an organization of aligned cell rows. The appendage fields are increasing in size, number of nuclei, and bulge prominently from the ventral surface of the segmenting ectoderm. The fused midgut anlagen have begun to spread dorsally and posteriorly under the ectoderm (Fig. 12d).

A split in the ventral midline begins to appear at this stage (Fig. 10d). As ventral flexure continues, the split extends anteriorly and is similar in appearance to the split ventral midline observed in *Orchestia cavimana* (Gerberding and Scholtz, 1999, 2001). The developing stomodeum and two lateral esophageal projections are visible medially at the level of An1 (Fig. 10d). The para-

gnaths can be seen developing at the medial edges of the mandible primordia (Fig. 10d).

At 96 h, An2 is composed of three elements. The two visible elements of T1 have continued to extend. T3 is composed of three elements, and T5 is composed of two elements (Fig. 11a).

S20 Stage 20 (112 h; 44.8%)

Posterior narrows, morphologically distinct telson appears

Engrailed expression: Ocular spots, An1, An2, Mn, Mx1, Mx2, T1, T2, T3, T4, T5, T6, T7, T8, A1, A2, A3, A4, A5, A6, telson

In vivo. At 112 h the posterior paddle has significantly narrowed and limb buds are visible on the abdomen (Fig. 13a). The developing telson is visible at the posterior end of the embryo. Due to the flexure of the embryo and continued growth, the telson is oriented anteriorly and projects towards the first thoracic segment (Fig. 13a). The head segments have returned to a more ventral aspect. An area of clearing is visible in the dorsal part of the dorsal organ (Fig. 13a). The germ cell clusters are visible in the lower hemisphere of the midgut anlagen and are beginning to migrate dorsally in the embryo (Fig. 13a). The developing midgut can be seen as an organized epithelial sheet spreading over the yolk.

Fixed + DAPI. In DAPI preparations at 112 h the antennae arc prominently anteriorly and dorsally towards the dorsal organ. The labrum is visible projecting medially and posteriorly between the antennae (Fig. 13a). Just posterior of the labrum the lower edge of the stomodeum is visible as a raised medial ridge. The first and second maxillae appendage fields appear to make contact with the ventral surface of the egg membranes. The proximal base of each of the anterior thoracic appendage fields have begun to branch (T2-T6 coxal plates). The dorsal edges of the midgut anlagen fuse and posterior envelopment of the yolk continues to progress (the leading edge can be seen just above T4 in Fig. 13a).

By 112 h, An2 has undergone a rapid elongation and is composed of five proximal elements forming the peduncle and one distal flagella element. An2 grows along a dorsal vector across the developing head. T1 and T5 are composed of three visible endopodal elements. The basis of T1 has begun to generate a new P-D axis medially. T3 is composed of four visible endopodal elements (Fig. 11a).

S21 Stage 21 (120 h; 48%)

Hindgut proctodeum becomes visible

In vivo. At 120 h, all abdominal segments possess visible limb buds. The telson now projects forward to the Mn segment. The hindgut proctodeum is just becoming visible at the posterior terminus (Fig. 13b). The clearing at the position of the dorsal organ appears to increase in size (Fig. 13b). Laterally, the midgut appears as a wedge

with a broad dorsal aspect that progressively narrows ventrally (Fig. 13b). The germ cell clusters continue to be visible in the lower portion of the midgut wedge (Fig. 13b).

Fixed + DAPI. In DAPI preparations the labrum has nearly completed its posterior extension and is visible just anterior to the paragnaths (Fig. 13b). The forming hindgut proctodeum is clearly visible as a wedge-shaped ridge of nuclei just anterior to the embryo's posterior terminus (Fig. 13b). The split midline is most prominent along the thoracic ventral midline at this stage (Fig. 8f). After this stage the split ventral midline will close as the ventral ganglia begin to mature and fuse.

At 120–132 h, An2 continues to extend in length as individual elements continue to enlarge. T1 is composed of four elements. In addition, two nascent P-D axes forming the endites are being generated ventrally, one from the proximalmost element and one from the second element of the endopodal appendage axis (Fig. 11a). T3 is composed of seven elements along the endopodal P-D axis: coxa, basis, ischium, merus, carpus, propodus, and dactyl. The coxa possesses two nascent P-D axes, both generating dorsal appendage branches (proximally the coxal plate and distally the epipod gill). The ischium is wedge-shaped with the narrow end oriented anteriorly, thus giving the T3 appendage its characteristic anterior orientation (also a diagnostic feature for T2). In addition, the propodus has become expanded laterally (also a diagnostic feature for T2). All seven endopodal elements of T5 are visible and the coxa begins to bud two nascent P-D axes (Fig. 11a).

S22 Stage 22 (132 h; 52.8%)

Limb bud elongation stage

In vivo. The midgut completely envelops the remaining yolk.

Fixed + DAPI. The ventral midline is no longer split, as the left and right halves have closed back together by this stage.

At 132 h the fourth element of the peduncle of An2 undergoes a distinct change in shape, narrowing at its proximal end and expanding at its distal end. The two endites of T1 are beginning to elongate and the principal P-D axis of T1 is now composed of five elements. T3 is continuing to elongate and both dorsal appendage branches are increasing in size. The endopod of T5 now possesses a complete complement of seven elements: coxa, basis, ischium, merus, carpus, propodus, and dactyl and both dorsal appendage branches (coxal plate and epipod gill) are well formed (Fig. 11a).

S23 Stage 23 (144 h; 57.6%)

Digestive cecae begin to extend, yolk granules clear from the head, tergites and coxal plates visible

In vivo. At ~144 h the developing body wall tergites are visible through the eggshell. Dorsal closure of the ectoderm over the gut appears to be nearly complete. The coxal plate (dorsalmost branch) of the thoracic appendages (T2–T8) becomes visible laterally. The cephalon

is completely clear of yolk granules (Fig. 13c). The antennae now arc posteriorly along the ventral margin of the head capsule. The clearing associated with the dorsal organ projects posteriorly as a narrow strip along the dorsalmost aspect of the embryo (Fig. 13c). The germ cell clusters have taken positions on the anterior medial-lateral and anterior dorsal region of each of the bilateral paired cecae rudiments that are beginning to project posteriorly (Fig. 13c).

The digestive cecae are major secretory organs consisting of a pair of blind tubes that open directly into the anterior end of the medial midgut. They are thought to play a role in nutrient adsorption and storage (reviewed in Schmitz, 1992). At 144 h the anterior medial cecum rudiment begins to project anteriorly and dorsally into the medial portion of the head capsule. The two bilaterally positioned cecae rudiments simultaneously begin to project posteriorly from the ventral posterior aspect of the wedge-shaped midgut Anlagen (Fig. 13c). The extension of the cecum rudiments occurs in unison and is characterized by a series of peristaltic, muscular contractions that initiate alternately from the anterior and posterior ends of the rudiment. Each contractile wave increases the overall length and girth of the cecum. Ultimately, the two cecae extend to very near the posterior limit of the embryo. The initial peristaltic wavefronts are of short duration (traveling the length of a small, short rudiment), whereas the terminal wavefront durations can be several minutes (traveling the length of a fully extended cecum). This process of extension requires ~20 h to reach completion.

Fixed + DAPI. In DAPI preparations at 144 h the density of nuclei along the dorsal aspect of the embryo is beginning to increase and resolve into distinct segmental bands.

At 144 h, An2 begins to conform to its final cylindrical uniramous shape. The T1, T3, and T5 appendages are continuing to increase in size (Fig. 11a).

S24 Stage 24 (155 h; 62%)

Midpoint of digestive cecae extension

In vivo. The cephalon has acquired a rounded shape. The abdomen is well formed. The lateral and dorsal body wall tergites are clearly visible. The bilateral digestive cecae have progressed approximately midway and are nearing the abdomen (Fig. 13d). The yolk deposits within the digestive cecum visibly change color as the granules are broken down (Fig. 13d).

Fixed + DAPI. The cephalon has the highest density of visible nuclei with the notable exception of the forming eye fields (Fig. 13d). Segmentation is apparent throughout the lateral and dorsal body wall and the thoracic coxal plates are clearly visible (Fig. 13d).

S25 Stage 25 (168 h; 67.2%)

Digestive cecae extension complete

In vivo. At the end of the digestive cecae extension process, most of the remaining yolk has been transferred

from the developing medial midgut to the digestive cecae. The midgut remains visible medially along the dorsal midline between the digestive cecae sacs as a thin yolk colored strip.

Fixed + DAPI. At 168 h, An2 has taken on a cylindrical shape. The An2 elements appear to decrease in size along the P-D axis (Fig. 11a). T1 has acquired its complete complement of seven elements (coxa, basis, ischium, merus, carpus, propodus, and dactyl) along the principal P-D axis and has begun to acquire its characteristic shape. Both ventral appendage branches of T1 continue to increase in size. T3 begins to acquire its final shape in which the anterior bend in the ischium is pronounced and the laterally expanded face of the propodus is enhanced. The T3 dactyl begins to develop its posterior orientation, which will align with the expanded distal ridge of the propodus. The dorsalmost branch, the coxal plate, becomes expanded laterally. The remaining dorsal branch, the epipod gill, becomes laterally expanded and oriented both posteriorly and ventrally, thus occupying a position ventral to the endopod. T5 also begins to acquire its final shape in which the coxal plate becomes laterally expanded and the gill takes on a similar orientation as in T3 (Fig. 11a).

S26 Stage 26 (180 h; 72%)

White eyes and beating heart

In vivo. The eye fields become distinctly visible as two bilaterally symmetric, whitish hued clusters of rhabdomeres (Fig. 13e). The tubular heart of *Parhyale hawaiiensis* is located along the dorsal thoracic region from T2-T7 and begins to visibly beat. It is a bilaterally symmetric, single-chambered structure positioned along the midline of the embryo, dorsal to the midgut (Divakaran, 1975). Yolk stores in the digestive cecum begin to diminish.

Fixed + DAPI. The appendages appear to be crowded into the curled embryo and begin to narrow significantly. Secretion of cuticle is visually detectable at this stage. The spatial organization of cells comprising the coxal plates and tergites is clearly visible (Fig. 13e).

S27 Stage 27 (192 h; 76.8%)

Red eyes

In vivo. Pigment cells that surround the whitish rhabdomeres begin to accumulate a deep red color at 192 h of development.

Fixed + DAPI. At 192 h, An2 has begun to visibly cuticularize and the diameter of the peduncular and flagellar elements continues to narrow as An2 achieves its final morphology. The T1, T3, and T5 appendages continue to increase in size.

S28 Stage 28 (216 h; 86.4%)

Yellow cuticle

In vivo. At 216 h the embryo cuticle acquires a yellow-gold appearance. Detection of gene expression becomes problematic as the cuticle thickens. The diges-

tive cecae are significantly depleted of yolk stores (Fig. 13f). The heart is beating strongly.

Fixed + DAPI. Most DAPI preparations at this stage, and later, burst through the eggshell during processing (Fig. 13f). The appendages have largely acquired their unique morphologies; for example, T1 has been incorporated into the buccal mass (Fig. 13f).

At 216 h, An2 is becoming heavily cuticularized. The T1, T3, and T5 appendages have acquired their final morphology and are also becoming heavily cuticularized.

S29 Stage 29 (230 h; 92%)

Muscular twitching

In vivo. Muscular twitching of appendages and body are readily visible through the egg shell.

Fixed + DAPI. Although An2 has acquired its final shape at S28, the appendage has continued to grow. The T1 appendage appears to have acquired both its final hatching morphology and hatching setae. The proximal endite of T1 has formed a plate-like structure, the medial endite has formed a toothed comb, and the distal portion of the endopodal branch (palp) is strongly curved medially and terminates with a hook-like structure (see Fig. 11a, ~240 h). The T3 and T5 appendages have acquired hatching setation and morphology.

S30 Stage 30 (250 h; 100%)

Hatching

In vivo. Hatching occurs at ~250 h of development. Immediately prior to hatching the embryo is in a constant state of coordinated motion. In addition, the embryo increases substantially in size immediately prior to and during hatching, most likely via active uptake of water. Soon after breaking free of the eggshell, hatchlings will undergo a molt and revert to a smaller size.

DISCUSSION

Embryonic staging systems, including the most recent arthropod systems, have historically taken two principal descriptive forms: 1) age-dependent staging using absolute time or percent of development, or 2) event-dependent staging (Campos-Ortega and Hartenstein, 1985; Hartenstein, 1993; Olesen and Walossek, 2000; Bentley *et al.*, 1979; Sandeman and Sandeman, 1991). We have attempted to combine both staging forms to facilitate the use of *Parhyale hawaiiensis* for a variety of developmental and comparative studies (Figs. 2, 7). Strict adherence to either an age or percentage staging system bearing a linear relationship to time would, by necessity, deemphasize the occurrence of important singular events during embryogenesis. For example, cleavage events that occur during the first 5% of development in *P. hawaiiensis* establish the primary axes of the developing embryo (Figs. 2-4) (Gerberding *et al.*, 2002). By the same token, a strict adherence to event staging would hamper comparative studies between related organisms in which synonymous, analogous, or homolo-

gous developmental events have a shifted temporal relationship with one another (Jeffery *et al.*, 2002). A comprehensive approach comprising a descriptive account of developmental events within an age-dependent framework, upon which the percentage of total developmental time has been mapped, will allow the maximum degree of flexibility and accuracy when planning and implementing developmental and comparative studies.

A particularly distinctive aspect of *Parhyale* development is the holoblastic cell cleavage pattern seen during early development. The eight-cell stage (S4) of *P. hawaiiensis* is described here (Figs. 3, 4) and the associated fate mapping of each of the eight blastomeres is described in Gerberding *et al.* (2002). The early establishment of distinct cell lineages in *P. hawaiiensis* allows for a wide range of experimental manipulations of both specific cell lineages and germ layers via microinjection and other perturbation techniques (i.e., Extavour, 2005). In addition, some variation in cleavage patterns (both in time and pattern) is observed in *Orchestia cavimana* (Wolff and Scholtz, 2002) and other amphipods (C. Babbitt, M. Modrell, and N.H. Patel, unpubl. data). Early holoblastic cleavage appears to be a general feature of amphipod embryogenesis (see Scholtz and Wolff, 2002), and thus future studies of these variations in timing and pattern of cell cleavage, and their resulting lineages, may perhaps be informative with regard to evolutionary patterns within the Amphipoda.

The current widespread use of several pan-specific antibodies makes the inclusion of the associated expression patterns highly desirable in staging systems. The monoclonal antibody to Engrailed (MAB4D9; Patel *et al.*, 1989b) allows for finer resolution of several patterning events along the A-P axis (Figs. 7, 8), as well as later patterning within the developing CNS (Duman-Scheel and Patel, 1999; Fig. 9). Similarly, the antibody to Distalless allows for a more detailed examination of the formation of appendage fields (Fig. 10). For example, Dll initiation in the d4 cell of developing *Parhyale hawaiiensis* parasegments (parasegment 3 and posterior; Figs. 6d, 10b,c) is slightly different than that observed in a related amphipod, *Orchestia cavimana*, and the isopod *Porcellio scaber* (Hejnal and Scholtz, 2004). Notably, the temporal dynamics of Dll expression in the mandibular segment of *P. hawaiiensis* (Fig. 10b,c) supports the hypothesis that Dll is required for patterning the crustacean mandibular primordia (Browne and Patel, 2000). Thus, the absence of Dll in the insect mandible is likely an automorphy of the insect lineage (Scholtz *et al.*, 1998).

The segmental organization of the arthropod head has been a formidable problem for biologists. Recently, the origin and segmental affiliation of the arthropod labrum has been reexamined (Haas *et al.*, 2001a,b; Boyan *et al.*, 2002; Eriksson *et al.*, 2003). An appendicular origin has been proposed based on homeotic transformation results in the flour beetle, *Tribolium* (Haas *et al.*, 2001b). The segmental affiliation of the labrum has been suggested to be on the intercalary segment based on innervation data in both *Tribolium* and the grasshopper,

Schistocerca (Haas *et al.*, 2001a; Boyan *et al.*, 2002). In this scenario the stomodeum would have its origin at the intercalary/mandibular segment boundary (Haas *et al.*, 2001a). Eriksson *et al.* (2003), however, suggest support for an ancestral anterior terminal position for the stomodeum based on development in the Onychophoran *Euperipatoides*, a basal arthropod. In *Euperipatoides* the stomodeum appears first at an anterodorsal position and migrates ventroposteriorly during development. Weygoldt (1958) also describes a ventroposterior migration of both the labrum and the stomodeum in the amphipod *Gammarus pulex*.

The origin, segmental affiliation, and morphogenesis of both the labrum and stomodeum were followed in *P. hawaiiensis* (Figs. 10, 13). The labrum expresses Dll strongly at S15 (Fig. 10b), supporting an appendicular origin. However, the position of the labrum first appears anterior and medial of the En and Dll ocular expression domains. Thus, the positional origin and segmental affiliation of the labrum is anterior of the first antennal segment, contrary to the model suggested by Haas *et al.* (2001a,b). The ectodermal origin of the labrum precedes CNS innervation and thus calls into question the use of tritocerebral innervation patterns as the sole means to determine the positional origin and segmental affiliation of the labrum (Boyan *et al.*, 2002). The stomodeum is readily visible via DAPI staining at S19 posterior of the labrum (Fig. 10d). At this stage the anterior half of the stomodeum is in the medial region of the An1 segment and the posterior half of the stomodeum is in the anterior medial region of the An2 segment (Fig. 10d). As development continues, both the labrum and the stomodeum move posteriorly. The labrum will continue to project ventral and posterior serving as the "upper lip" of the stomodeum. The entrance of the stomodeum later in development will largely be at the level of the mandibles, which will flank the esophageal opening.

As illustrated in Figure 11, amphipods such as *P. hawaiiensis* display remarkable morphological variation in the appendages along their anterior/posterior axis. The appendage staging data provided here will be valuable for future studies of appendage development and evolution. For example, either in studies designed to understand possible roles of homeotic genes in crustacean appendage evolution or investigations into molecular mechanisms used to generate branched appendages (e.g., Giorgianni and Patel, 2004; Hejnal and Scholtz, 2004).

In summary, we have described a number of aspects of the life history and development of *Parhyale hawaiiensis* that make it particularly attractive for developmental and evolutionary studies. It is a widespread, common, circum-tropical species that breeds year-round. The adults are relatively small and are easy to maintain in dense laboratory cultures. Individual broods of synchronous eggs can be easily removed from females and maintained in small volumes of seawater until hatching. Complete embryogenesis of *P. hawaiiensis* at 26°C requires 10 days, and the egg-to-egg generation time is 7–8 weeks when maintained at 26–28°C. While the yolk remains opaque, it

quickly becomes sequestered towards the center of the egg and eventually into the developing midgut; the embryo itself is optically clear. The embryos are robust and highly resistant to environmental variations in temperature and salinity and are suitable for a wide range of experimental manipulations. Additionally, the embryos are direct developers and the hatchlings are morphologically similar to adults. The staging system presented here should be beneficial to all further developmental studies of *P. hawaiiensis* and related amphipods.

MATERIALS AND METHODS

Amphipod Culture

The laboratory population of *Parhyale hawaiiensis* originated from the John G. Shedd Aquarium (Chicago, IL) in 1997 as an isolate from their marine filtration system, and thus was "preselected" as a crustacean species that requires minimal care. Laboratory breeding colonies are maintained in shallow plastic trays (47 × 33 × 12 cm containing 16 L of saltwater) at ~26°C. Individual trays are covered with clear Plexiglas and illumination is provided from ambient room illumination and fluorescent strip lighting with a day/night cycle of ~12/12 h. Water is circulated within trays by submersible pumps (40–150 US gal/h). Crushed coral substrate is provided as a thin bottom layer (1.5–2.5 cm) in each tray. Phosphate-absorbing resin (Phosguard, Seachem) is used to control accumulation of free phosphates. Either artificial salt (HW Marinemix) premixed in a 55 US gal container to a true specific gravity of 1.018–1.022 or filtered natural seawater is used. Each tray receives a 50% water change every week. Temperature is maintained by heating the room in which the tanks are located. Animals are maintained on a diet of algae wafers (Hikari), kelp powder/flakes (NOW), and a 1:1:1 liquid mixture of fatty acids (Selcon), plankton (MarineSnow), and vitamins (Multi-Vit, Hawaiian Marine).

For experimental manipulation of embryos, sexually mature pairs in amplexus are collected and placed in small dishes (13 × 18 × 8.5 cm containing 1 L of fresh seawater) overnight at 18°C. The following day, most of the males and females in amplexus have separated. The separation of the male and females occurs as the females molt (shed their old cuticle). Once the molt is complete, mature oocytes are released through the oviducts, fertilized, and deposited in the female's ventral brood pouch. At this time single-cell embryos are collected by immobilizing the adult female and opening the ventral brood pouch with forceps. In order to establish fairly precise time points for our staging system, synchronous embryos from single brood pouches were then placed in filter sterilized seawater (0.22 μm Millipore filter, Bedford, MA) in 35-mm Petri dishes and maintained in a high humidity chamber at 26°C until they reached specific time points for manipulation, dissection, and/or fixation.

Light Microscopy

All light micrographs were taken on either a Zeiss Stemi DRC dissecting microscope or a Zeiss Axiophot with a Kontron 3012 digital camera. For light microscopy, individual embryos were placed in shallow well slides with seawater and illuminated with intense side lighting.

DAPI (4,6-Diamidino-2-phenylindole) Staining Alone

After live light microscopy and photography, individual embryos were fixed by boiling in 1× PBS (1.86 mM NaH₂PO₄; 8.41 mM Na₂HPO₄; 175 mM NaCl; pH 7.4) for several minutes (<7 min), then washed with methanol and incubated in 50% (v:v) glycerol/1× PBS containing 1 mg/ml DAPI overnight at 4°C for visualization of nuclei by fluorescence microscopy. The individual embryos were then rephotographed to match the live photos. Thus, for Figures 5, 12, and 13 image pairs are a light microscope picture of a living embryo and the matching DAPI image of the same embryo after fixation (relative orientation matched as closely as possible). This procedure was followed because light microscope images of chemically or heat-fixed embryos look quite different from live embryos (individual cells and structures are more clearly visible in live preparations than in fixed embryos with just light microscopy), and it is important to be able to stage living embryos for various experimental procedures.

Antibody Staining

Embryos that had been allowed to develop for specific periods of time were dissected and fixed for 20 min in a 9:1 (v:v) mixture of Hepes fixation buffer (100 mM Hepes, pH 6.9, 2 mM MgSO₄, and 1 mM EGTA) and 37% formaldehyde. Tungsten wire needles were used during fixation to remove extracellular membranes. Fixed embryos were then washed with PT (1× PBS, pH 7.4, and 0.1% Triton X-100) and stored in 100% methanol at –20°C. Antibody detection was performed as described in Patel (1994). All antibody incubations were done overnight at 4°C at the following concentrations: mouse MAb 4D9 anti-Engrailed (Patel *et al.*, 1989b) 1:1, rabbit anti-Distalless (Panganiban *et al.*, 1995) 1:100, HRP conjugated goat anti-mouse (Jackson ImmunoResearch, West Grove, PA) 1:300, HRP conjugated goat anti-rabbit (Jackson ImmunoResearch) 1:500. After histochemical DAB reactions, embryos were washed and incubated overnight at 4°C in 50% glycerol + 1 mg/ml DAPI solution. Embryos were then stored in 70% glycerol at –20°C.

ACKNOWLEDGMENTS

We thank Mark Q. Martindale, Danielle Liubicich, Melinda Modrell, Patricia M. Lee, Amy Maxmen, and two anonymous reviewers for providing critical comments that significantly improved this communication. We thank the John G. Shedd Aquarium, Chicago, IL, for

allowing us to collect *Parhyale hawaiiensis* from their marine filtration system; these collected animals are the founding population of all our cultures. NHP is an Investigator of the Howard Hughes Medical Institute.

LITERATURE CITED

- Barnard JL. 1965. Marine Amphipoda of atolls in Micronesia. *Proc U S Natl Mus* 117:459-551.
- Barnard JL, Karaman GS. 1991. The families and genera of marine gammaridean Amphipoda (except marine gammaroids). *Rec Aust Mus Suppl* 13:1-866.
- Bentley D, Keshishian H, Shankland M, Toroian-Raymond A. 1979. Quantitative staging of embryonic development of the grasshopper, *Schistocerca nitens*. *J Embryol Exp Morphol* 54:47-74.
- Boore JL, Collins TM, Stanton D, Daehler LL, Brown WM. 1995. Deducing the pattern of arthropod phylogeny from mitochondrial DNA rearrangements. *Nature* 376:163-165.
- Boore JL, Lavrov DV, Brown WM. 1998. Gene translocation links insects and crustaceans. *Nature* 392:667-668.
- Boyan GS, Williams JLD, Posser S, Braunig P. 2002. Morphological and molecular data argue for the labrum being non-apical, articulated, and the appendage of the intercalary segment in the locust. *Arthropod Struct Dev* 31:65-76.
- Browne WE, Patel NH. 2000. Molecular genetics of crustacean feeding appendage development and diversification. *Semin Cell Dev Biol* 11:427-435.
- Campos-Ortega JA, Hartenstein V. 1985. The embryonic development of *Drosophila melanogaster*. Berlin: Springer.
- Dana JD. 1853. Crustacea. Part II. United States Exploring Expedition 14:689-1618.
- Divakaran O, Pillai NK. 1975. The vascular system of *Parhyale hawaiiensis* (Amphipoda). *Acta Zool* 56:129-139.
- Divakaran O, Pillai NK. 1981. Functional morphology of the respiratory system of *Parhyale hawaiiensis* Dana (Crustacea: Amphipoda). *Proc Indian Nat Sci Acad B47:664-669*.
- Dohle W. 1970. Die Bildung und Differenzierung des postnauplialen Keimstreifs von *Diastylis rathkei* (Crustacea, Cumacea). *Zeit Morphol Tiere* 67:307-392.
- Dohle W. 1976. Die Bildung und Differenzierung des postnauplialen Keimstreifs von *Diastylis rathkei* (Crustacea, Cumacea). *Zoomorphologie* 235-277.
- Dohle W, Scholtz G. 1988. Clonal analysis of the crustacean segment: the discordance between genealogical and segmental borders. *Development* 104(Suppl):147-160.
- Dohle W, Scholtz G. 1997. How far does cell lineage influence cell fate specification in crustacean embryos? *Semin Cell Dev Biol* 8:379-390.
- Duman-Scheel M, Patel NH. 1999. Analysis of molecular marker expression reveals neuronal homology in distantly related arthropods. *Development* 126:2327-2334.
- Eernisse DJ. 1997. Arthropod and annelid relationships re-examined. In: Fortey RA, Thomas RH, editors. *Arthropod relationships*. London: Chapman and Hall. p 43-56.
- Eriksson BJ, Tait NN, Budd GE. 2003. Head development in the Onychophoran *Euperipatoides kanangrensis* with particular reference to the central nervous system. *J Morphol* 255:1-23.
- Extavour CG. 2005. The fate of isolated blastomeres with respect to germ cell formation in the amphipod crustacean *Parhyale hawaiiensis*. *Dev Biol* 277:387-402.
- Friedrich M, Tautz D. 1995. Ribosomal DNA phylogeny of the major extant arthropod classes and the evolution of myriapods. *Nature* 376:165-167.
- Gasca R, Haddock SHD. 2004. Associations between gelatinous zooplankton and hyperiid amphipods (Crustacea: Peracarida) in the Gulf of California. *Hydrobiologia* 530/531:529-535.
- Gerberding M, Scholtz G. 1999. Cell lineage of the midline cells in the amphipod crustacean *Orchestia cavimana* (Crustacea, Malacostraca) during formation and separation of the germ band. *Dev Genes Evol* 209:91-102.
- Gerberding M, Scholtz G. 2001. Neurons and glia in the midline of the higher crustacean *Orchestia cavimana* are generated via an invariant cell lineage that comprises a median neuroblast and glial progenitors. *Dev Biol* 235:397-409.
- Gerberding M, Browne WE, Patel NH. 2002. Cell lineage analysis of the amphipod crustacean *Parhyale hawaiiensis* reveals an early restriction of cell fates. *Development* 129:5789-5801.
- Giorgianni MW, Patel NH. 2004. Patterning of the branched head appendages in *Schistocerca americana* and *Tribolium castaneum*. *Evol Dev* 6:402-410.
- Giribet G, Edgecombe GD, Wheeler WC. 2001. Arthropod phylogeny based on eight molecular loci and morphology. *Nature* 413:157-161.
- Gonzalez-Crespo S, Morata G. 1996. Genetic evidence for the subdivision of the arthropod limb into coxopodite and telopodite. *Development* 122:3921-3928.
- Haas MS, Brown SJ, Beeman RW. 2001a. Pondering the procephalon: the segmental origin of the labrum. *Dev Genes Evol* 211:89-95.
- Haas MS, Brown SJ, Beeman RW. 2001b. Homeotic evidence for the appendicular origin of the labrum in *Tribolium castaneum*. *Dev Genes Evol* 211:96-102.
- Hartenstein V. 1993. Atlas of *Drosophila* development. Cold Spring Harbor, NY: Cold Spring Harbor Laboratory Press.
- Hejnol A, Scholtz G. 2004. Clonal analysis of Distal-less and engrailed expression patterns during early morphogenesis of uniramous and biramous crustacean limbs. *Dev Genes Evol* 214:473-485.
- Hwang UW, Friedrich M, Tautz D, Park CJ, Kim W. 2001. Mitochondrial protein phylogeny joins myriapods with chelicerates. *Nature* 413:154-157.
- Jeffery JE, Richardson MK, Coates MI, Bininda-Emonds ORP. 2002. Analyzing developmental sequences within a phylogenetic framework. *Syst Biol* 51:478-491.
- Kamaltynov RM. 1999. On the evolution of Lake Baikal Amphipods. *Crustaceana* 72:921-931.
- Langenbeck C. 1898. Formation of the germ layers in the amphipod *Microdeutopus gryllotalpa* Costa. *J Morphol* 14:301-336.
- Lindeman D. 1991. Natural history of the terrestrial amphipod *Cerorchestia hyloraina* Lindeman (Crustacea: Amphipoda; Talitridae) in a Costa Rican cloud forest. *J Nat Hist* 25:623-638.
- Meschenmoser M. 1989. Ultrastructure of the embryonic dorsal organ of *Orchestia cavimana* (Crustacea, Amphipoda); with a note on localization of chloride and on the change in calcium-deposition before the embryonic moult. *Tissue Cell* 21:431-442.
- Myers AA. 1985. Shallow-water, coral reef and mangrove Amphipoda (Gammaridea) of Fiji. *Rec Aust Mus Suppl* 5:1-143.
- Olesen J, Walossek D. 2000. Limb ontogeny and trunk segmentation in *Nebalia* species (Crustacea, Malacostraca, Leptostraca). *Zoomorphology* 120:47-64.
- Panganiban G, Sebring A, Nagy L, Carroll S. 1995. The development of crustacean limbs and the evolution of arthropods. *Science* 270:1363-1366.
- Panganiban G, Irvine SM, Lowe C, Roehl H, Corley LS, Sherbon B, Grenier JK, Fallon JE, Kimble J, Walker M, Wray GA, Swalla BJ, Martinale MQ, Carroll SB. 1997. The origin and evolution of animal appendages. *Proc Natl Acad Sci U S A* 94:5162-5166.
- Patel N. 1994. Imaging neuronal subsets and other cell types in whole mount *Drosophila* embryos and larvae using antibody probes. *Methods Cell Biol* 44:445-487.
- Patel NH, Kornberg TB, Goodman CS. 1989a. Expression of engrailed during segmentation in grasshopper and crayfish. *Development* 107:201-212.
- Patel NH, Martin-Blanco E, Coleman KG, Poole SJ, Ellis MC, Kornberg TB, Goodman CS. 1989b. Expression of engrailed proteins in arthropods, annelids, and chordates. *Cell* 58:955-968.
- Poltermann M, Hop H, Falk-Peterson S. 2000. Life under Arctic sea ice — reproduction strategies of two sympatric (ice-associated) amphipod species, *Gammarus wilkitzkii* and *Apherusa glacialis*. *Mar Biol* 136:913-920.
- Poovachiranon S, Boto K, Duke N. 1986. Food preference studies and ingestion rate measurements of the mangrove amphipod *Parhyale hawaiiensis* (Dana). *J Exp Mar Biol Ecol* 98:129-140.

- Regier JC, Shultz JW. 1997. Molecular phylogeny of the major arthropod groups indicates polyphyly of crustaceans and a new hypothesis for the origin of hexapods. *Mol Biol Evol* 14:902-913.
- Sandeman R, Sandeman D. 1991. Stages in the development of the embryo of the fresh-water crayfish *Cherax destructor*. *Roux's Arch Dev Biol* 200:27-37.
- Schmitz EH. 1992. Amphipoda. In: Harrison FW, editor. *Microscopic anatomy of invertebrates*. New York: Wiley-Liss. p 443-528.
- Scholtz G. 1990. The formation, differentiation and segmentation of the post-naupliar germ band of the amphipod *Gammarus pulex* L. *Proc R Soc Lond B* 239:163-211.
- Scholtz G. 1992. Cell lineage studies in the crayfish *Cherax destructor* (Crustacea, Decapoda): germ band formation, segmentation, and early neurogenesis. *Roux's Arch Dev Biol* 202:36-48.
- Scholtz G, Dohle W. 1996. Cell lineage and cell fate in crustacean embryos — a comparative approach. *Int J Dev Biol* 40:211-220.
- Scholtz G, Wolff C. 2002. Cleavage, gastrulation, and germ disc formation of the amphipod *Orchestia cavimana* (Crustacea, Malacostraca, Peracarida). *Contrib Zool* 71:9-28.
- Scholtz G, Dohle W, Sandeman RE, Richter S. 1993. Expression of engrailed can be lost and regained in cells of one clone in crustacean embryos. *Int J Dev Biol* 37:299-304.
- Scholtz G, Patel NH, Dohle W. 1994. Serially homologous engrailed stripes are generated via different cell lineages in the germ band of amphipod crustaceans (Malacostraca, Peracarida). *Int J Dev Biol* 38:471-478.
- Scholtz G, Mittmann B, Gerberding M. 1998. The pattern of Distal-less expression in the mouthparts of crustaceans, myriapods and insects: new evidence for a gnathobasic mandible and the common origin of Mandibulata. *Int J Dev Biol* 42:801-810.
- Schram FR. 1986. *Crustacea*. Oxford: Oxford University Press.
- Shedler M, Van Dover CL, Shank TM. 2000. Structure and function of *Halice hesmonectes* (Amphipoda: Pardaliscidae) swarms from hydrothermal vents in the eastern Pacific. *Mar Biol* 136:901-911.
- Sherbakov DY, Kamaltynov RM, Ogarkov OB, Vainola R, Vainio JK, Verheyen E. 1999. On the phylogeny of Lake Baikal amphipods in the light of mitochondrial and nuclear DNA sequence data. *Crustaceana* 72:911-919.
- Shoemaker CR. 1956. Observations on the amphipod genus *Parhyale*. *Proc U S Natl Mus* 106:345-358.
- Vainola R, Kamaltynov RM. 1999. Species diversity and speciation in the endemic amphipods of Lake Baikal: molecular evidence. *Crustaceana* 72:945-956.
- Vinogradov ME, Volkov AF, Semenova TN. 1996. *Hyperiid amphipods (Amphipoda, Hyperiidea) of the world oceans*. Washington, DC: Smithsonian Institution Libraries.
- Weygoldt P. 1958. Die Embryonalentwicklung des Amphipoden *Gammarus pulex pulex* (L.). *Zool Jb Anat* 77:51-110.
- Wolff C, Scholtz G. 2002. Cell lineage, axis formation, and the origin of germ layers in the amphipod crustacean *Orchestia cavimana*. *Dev Biol* 250:44-58.